# An inter-comparison of Deep Chlorophyll Maxima characteristics from 30S to 74S and their contribution to Net Primary Production

Clara R Vives[1], Christina Schallenberg[2], Peter G. Strutton[3], Jørgen Bendtsen[4], Katherine Richardson[5], and Philip W Boyd[6]

[1]Institute for Marine and Antarctic Studies, University of Tasmania, Hobart, TAS, Australia.
[2]CSIRO Environment
[3]University of Tasmania
[4]University of Copenhagen
[5]Center for Macroecology, Evolution and Climate, Globe Institute, University of Copenhagen, 2100 Copenhagen O, Denmark
[6]Institute for Marine and Antarctic Studies

August 20, 2024

### Abstract

Subsurface accumulations of chlorophyll, also known as deep chlorophyll maxima (DCMs), have been studied in the tropical and temperate oceans for decades, but they have received less attention in the Southern Ocean. Their formation and maintenance are still under debate, as is their contribution to phytoplankton biomass and net primary productivity (NPP). Recently, the application of satellite-based NPP algorithms to data from biogeochemical (BGC)-Argo floats has improved vertically-resolved NPP estimates. Using this new approach on 247 BGC-Argo floats, we report (1) subsurface (below the mixed layer) estimates of NPP, (2) the contribution of subsurface NPP to total NPP, and (3) the influence of DCMs and deep biomass maxima (DBMs, based on particulate backscatter) on (1) and (2). We compare and contrast trends in adjacent latitudinal bands in the southern hemisphere, south of 30°S, from nitrate-limited oligotrophic waters to iron-limited high-nutrient, low-chlorophyll (HNLC) regions. This comparison of pervasive DCMs in oligotrophic waters with the same features in HNLC waters reveals differences in seasonality of DCM occurrence and their contribution to total NPP. Unlike oligotrophic DCMs, HNLC DCMs occur only during spring and summer, and their contribution to total NPP decreases from ~40% to ~25% through the productive season, likely linked to the availability of iron and silicate. When DCMs are present but not accounted for, up to 45% of NPP is not quantified. Our results highlight the importance of understanding the vertical structure of phytoplankton stocks and productivity, with direct impacts on global NPP estimates and, ultimately, the biological carbon pump.

### Hosted file

`ms_Vivesetal.docx` available at https://authorea.com/users/815843/articles/1216629-an-inter-comparison-of-deep-chlorophyll-maxima-characteristics-from-30s-to-74s-and-their-contribution-to-net-primary-production

### Hosted file

`SI_Vivesetal.docx` available at https://authorea.com/users/815843/articles/1216629-an-inter-comparison-of-deep-chlorophyll-maxima-characteristics-from-30s-to-74s-and-their-contribution-to-net-primary-production

# An inter-comparison of Deep Chlorophyll Maxima characteristics from 30°S to 74°S and their contribution to Net Primary Production

Clara R. Vives[1,2,3*], Christina Schallenberg[4,5], Peter G. Strutton[1,2,6], Jørgen Bendtsen[3], Katherine Richardson[7], Philip W. Boyd[1,5,6]

[1]Institute for Marine and Antarctic Studies, University of Tasmania, Hobart, TAS, Australia.
[2]Australian Research Council Centre of Excellence for Climate Extremes, University of Tasmania, Hobart, TAS, Australia.
[3]Globe Institute, Section for Geobiology, University of Copenhagen, DK-1350 Copenhagen K, Denmark
[4]CSIRO Environment, Hobart, Tasmania, Australia
[5]Australian Antarctic Program Partnership, Institute for Marine and Antarctic Studies, University of Tasmania, Hobart, TAS, Australia.
[6]Australian Centre for Excellence in Antarctic Science, Institute for Marine and Antarctic Studies, University of Tasmania, Hobart, TAS, Australia.
[7]Center for Macroecology, Evolution and Climate, Globe Institute, University of Copenhagen, 2100 Copenhagen O, Denmark

*Correspondence: Clara R. Vives, clara.rodriguezvives@utas.edu.au

Key words:
Deep chlorophyll maxima, deep biomass maxima, net primary production, subtropical water-mass, Southern Ocean, BGC-Argo floats

## Key points

- Deep chlorophyll and biomass maxima occur across the Southern Ocean (>30°S), particularly in oligotrophic regions and in summer.
- Deep chlorophyll maxima in oligotrophic versus iron-limited waters show differences in seasonality and their contribution to production.

- When deep chlorophyll maxima are not accounted for up to 45% of net primary production is missed.

## Abstract

Subsurface accumulations of chlorophyll, also known as deep chlorophyll maxima (DCMs), have been studied in the tropical and temperate oceans for decades, but they have received less attention in the Southern Ocean. Their formation and maintenance are still under debate, as is their contribution to phytoplankton biomass and net primary productivity (NPP). Recently, the application of satellite-based NPP algorithms to data from biogeochemical (BGC)-Argo floats has improved vertically-resolved NPP estimates. Using this new approach on 247 BGC-Argo floats, we report (1) subsurface (below the mixed layer) estimates of NPP, (2) the contribution of subsurface NPP to total NPP, and (3) the influence of DCMs and deep biomass maxima (DBMs, based on particulate backscatter) on (1) and (2). We compare and contrast trends in adjacent latitudinal bands in the southern hemisphere, south of 30°S, from nitrate-limited oligotrophic waters to iron-limited high-nutrient, low-chlorophyll (HNLC) regions. This comparison of pervasive DCMs in oligotrophic waters with the same features in HNLC waters reveals differences in seasonality of DCM occurrence and their contribution to total NPP. Unlike oligotrophic DCMs, HNLC DCMs occur only during spring and summer, and their contribution to total NPP decreases from ~40% to ~25% through the productive season, likely linked to the availability of iron and silicate. When DCMs are present but not accounted for, up to 45% of NPP is not quantified. Our results highlight the importance of understanding the vertical structure of phytoplankton stocks and productivity, with direct impacts on global NPP estimates and, ultimately, the biological carbon pump.

## Plain Language Summary

Climate model projections suggest that ocean warming will cause changes in the vertical structure of ocean layers. This will likely have an effect on how photosynthetic plankton (phytoplankton) are distributed with depth. Subsurface accumulations of phytoplankton biomass, and pigments like chlorophyll, are characteristic of a stratified ocean. These deep chlorophyll or biomass peaks are referred to as deep chlorophyll or biomass maxima. In the waters south of 30°S they are less well studied than in the northern hemisphere, and their causes are still under debate. The significance of deep chlorophyll maxima and their influence on net primary production (the amount of ocean photosynthesis minus respiration) has never been measured for the Southern Ocean on a large scale. Using data from autonomous robotic floats, we calculate the contribution of deep chlorophyll maxima to net primary production. We show that when deep chlorophyll and biomass maxima occur in nitrate-limited waters, they contribute significantly to total ocean productivity. In iron-limited waters, deep chlorophyll maxima occur only in spring and summer, and their contribution to production decreases towards the end of the summer, as light levels decline. Accounting for subsurface accumulations of phytoplankton is critical for calculating net primary production through the euphotic zone.

## 1. Introduction

The Southern Ocean is a high-nitrate low-chlorophyll (HNLC) area, predominantly iron-limited (Martin et al. 1990; Boyd et al. 2007), where phytoplankton production plays a central role in the biological carbon pump and functioning of the marine ecosystem (Boyd and Trull 2007, Henson et al. 2012, Boyd 2015; Gruber et al., 2019). Net primary production (NPP) is the difference between the gross particulate organic carbon produced by marine autotrophs and the respiration of their carbon products (Huang et al., 2021). NPP can therefore be described as the organic carbon available for growth, and it is the most widely used variable when quantifying ocean productivity (Westberry et al. 2023). Marine NPP occurs in the sunlit upper ocean and accounts for ~50% of the global total (Field et al. 1998), although the uncertainty range in the ocean is large (Tagliabue et al., 2021). As increases in stratification due to warming are expected in the Southern Ocean (Bindoff et al., 2019), understanding the patterns in the vertical structure of NPP and the contribution of subsurface production is important, to be able to predict how ocean productivity and the biological carbon pump will be affected by climate change. However, the measurement of depth-resolved NPP in the ocean requires time and resources, resulting in sparse data sets, especially in the Southern Ocean.

The development of satellite-based algorithms, hereafter referred to as models, to derive NPP has been essential to the study of productivity in remote areas. The large temporal and spatial resolution of these data sets have been necessary to quantify long-term changes in biological production globally since the 1990s (Platt and Sathyendranath, 1988; Longhurst et al., 1995; Behrenfeld and Falkowski, 1997; Behrenfeld et al., 2005). Satellite measurements are restricted to the surface (~10-50m depth) of the ocean, and it is challenging for satellite-based models to extrapolate NPP to its maximum depth (typically the base of the euphotic zone). As the calculated vertical distribution of chl is based on algorithms using surface ocean color, there is also considerable uncertainty regarding future ocean estimates. More recently, NPP models like the Carbon-based Productivity Model (CbPM; Behrenfeld et al. 2005; Westberry et al., 2008) have been combined with *in situ* data from Biogeochemical (BGC)-Argo floats in the North Atlantic to estimate depth-resolved NPP using observations rather than the assumed depth distributions of carbon and chlorophyll (Estapa et al., 2019; Long et al., 2021; Yang et al. 2021; Bendtsen et al. 2023). Using this methodology researchers have been able to reproduce vertical NPP structure derived from depth-resolved $^{14}C$ incubation measurements in the Southern Ocean (Arteaga et al., 2022). Taking the approach one step further, Arteaga et al. have shown that the CbPM satellite estimates of NPP improve for the Southern Ocean south of 30°S if the ferricline depth (Southern Ocean average = 333m) is used to model nutrient limitation, rather than the nitracline.

Deep chlorophyll maxima (DCMs) are subsurface accumulations of chlorophyll, first observed in oligotrophic waters (Cullen, 1982). They are frequently-observed features in stratified waters, well-studied in macronutrient limited temperate regions (Estrada et al., 1993; Cullen et al., 1995; Fennel and Boss, 2003; Longhurst, 2007; Richardson and Bendtsen, 2017), and their occurrence and characteristics are primarily linked to a favourable combination of light and nitrate to sustain a phytoplankton layer at depth (Letelier et al., 2004; Cullen, 2015; Richardson and Bendtsen, 2019). DCMs have recently received more attention in the Southern Ocean (Baldry et al., 2020; Cornec et al., 2021a; Boyd et al. 2024). In the Southern Ocean, DCMs can form as a result of photoacclimation (Baldry et al., 2020; Cornec et al., 2021), where phytoplankton increase their cellular chlorophyll content in response to low light at depth (Geider et al., 1997; Westberry et al., 2016; Graff et al., 2019). Sporadic influx of nutrients, like the resupply of iron (Trull et al., 2001) from depth via eddies for example (Uchida et al., 2020), or silicate (Parslow et al., 2001), may also drive DCM formation in the Southern Ocean (Cornec et al., 2022; Strutton et al., 2023). DCMs can also coincide with a subsurface accumulation of phytoplankton biomass (Cullen, 2015; Latasa et al., 2016; Latasa et al., 2017), defined as deep biomass maxima (DBMs). DBMs tend to dominate in equatorial and subequatorial regions (0-10°) and tend to be proportional to photoacclimation-induced DCMs from 30° to high latitudes (Cornec et al., 20211). This study focuses on the DCMs in the Southern Ocean south of 30°S (Pinkerton et al. 2021; Cornec et al., 2021; Strutton et al., 2023; Boyd et al., 2024).

In the North Sea, subsurface summer blooms coinciding with pervasive DCMs have been shown to account for more production than the spring bloom (Richardson et al., 2000). Other studies in temperate and subtropical waters have shown that DCMs can significantly contribute to total water column production (Hickman et al., 2012; Fawcett et al., 2014; Richardson et al., 2014). A few studies to date have reported vertical patterns in phytoplankton biomass, DCM occurrence and subsurface blooms in regions including the North Atlantic (Lacour et al., 2017), Mediterranean Sea (Marañón et al., 2021), oligotrophic oceans (Mignot et al., 2014; Barbieux et al., 2019), and globally (Cornec et al., 2021; Bock et al., 2022). DCMs in the Southern Ocean have been found to be more prevalent at oligotrophic low-latitude waters, in the summer >40°S (Carranza et al., 2018; Baldry et al., 2020; Cornec et al., 2021), and be important potentially for downward carbon export (Boyd et al., 2024).

In this study, we use 247 BGC-Argo floats, south of 30°S, spanning 2012 to 2022, to estimate vertically-resolved NPP using the CbPM, following Arteaga et al. (2022). We then examine subsurface production (that is, all production below the mixed layer depth; MLD) for 3 cases: (1) DCM or DBM present; (2) DCM or DBM naturally absent; (3) DCM or DBM “removed”. Additionally, we quantify NPP occurring in the DCM and DBM. We calculate the subsurface contribution to the total integrated NPP and investigate the influence of DCM and DBM occurrence on this contribution. We compare results for water masses between the four Southern Ocean frontal zones, and across the southern hemisphere, from nitrate-limited oligotrophic waters (30-40°S), to iron-limited HNLC sub-Antarctic waters (40-60°S) to HNLC polar waters south of 60°S. Finally, we compare NPP estimates from floats and satellites, to assess whether satellite reconstructions of vertical NPP account for DCMs.

We find that when DCMs alone are present, NPP below the MLD contributes 59% of the total NPP on average across the entire dataset, and ~40% in iron-limited areas of the Southern Ocean. When DCMs coincide with a DBM, this contribution to total NPP increases to 66% overall. Furthermore, the contribution of subsurface NPP to total NPP varies spatially and seasonally, increasing at low latitudes (30-40°S) and during the summer, when DCMs are more prevalent. Omitting DCMs from the water column results in integrated NPP estimates of up to 45% lower NPP.

## 2. Methods

### 2.1. BGC-Argo float data

Data from 339 BGC-Argo floats from the Southern Ocean Carbon and Climate Observations and Modelling (SOCCOM) program were downloaded through the Australian Antarctic Division repository on 01-June-2022. This equated to a total of ~15,000 quality-controlled (QC) profiles south of 30°S, spanning 2012 to 2022. In this study we first divide the Southern Ocean into four zones, based on Bushinsky et al. (2017) using a 10-year Argo climatology of temperature and salinity, as follows: the sub-tropical zone (STZ) north of the sub-tropical front and south of 30°S, the sub-Antarctic zone (SAZ) between the sub-Antarctic and sub-tropical front, the polar Antarctic zone (PAZ) between the sea ice zone (SIZ) and polar Antarctic front, and the SIZ south of the maximum sea-ice extent (Figure 1). The maximum winter sea-ice extent was computed using daily sea-ice concentration products (25km resolution) from the Ocean and Sea Ice Satellite Application facility (OSI SAF) from the Copernicus website (https://cds.climate.copernicus.eu/cdsapp#!/dataset/satellite-sea-ice-concentration?tab=form), following Liniger et al., (2024). Because floats are quasi-Lagrangian and can cross regional boundaries when drifting, float profiles are divided into each zone based on location. This method to study large scale processes using fixed fronts has been widely used in the Southern Ocean (Bushinsky et al., 2017; Johnson et al., 2017; Llort et al., 2018; Arteaga et al., 2020; Su et al., 2022; Liniger et al., 2024). We then explore the latitudinal variability of our results using three bands based on nutrient-limitation: nitrate-limited oligotrophic waters (30-40°S), silicate and/or iron-limited HNLC sub-Antarctic waters (40-60°S), and iron-limited HNLC polar waters south of 60°S.

Data flagged as QC 4 (bad data) and 3 (bad data that are potentially correctable) were not included in our analyses (Johnson et al. 2017; Bittig et al. 2019). Two additional criteria were applied for removing profiles with insufficient data coverage: (1) the first pressure measurement should be in the upper 10 m, and (2) the upper 300 m of each profile should contain a minimum of 20 observations of all the variables used in the analysis. After applying these criteria, the total number of floats left for analysis was 247, of which 12,700 profiles were good for estimating NPP (Figure 1a). All floats were equipped with a CTD (for salinity, temperature and pressure), a nitrate sensor, and bio-optical sensors for fluorescence-derived chlorophyll *a* (chl, used to identify DCMs) and particulate backscatter at 700nm ($b_{bp}$, used to identify DBMs). SOCCOM floats have a sampling period of 10 days. The vertical resolution of profiles decreases with depth, from 5m in the upper 100m, to 10m below 100m, to 20m below 360m and 50m between 400m to 2000m. Vertical profiles were extrapolated to the surface, and chl and $b_{bp}$ interpolated from 0 to 300m with 1m resolution.

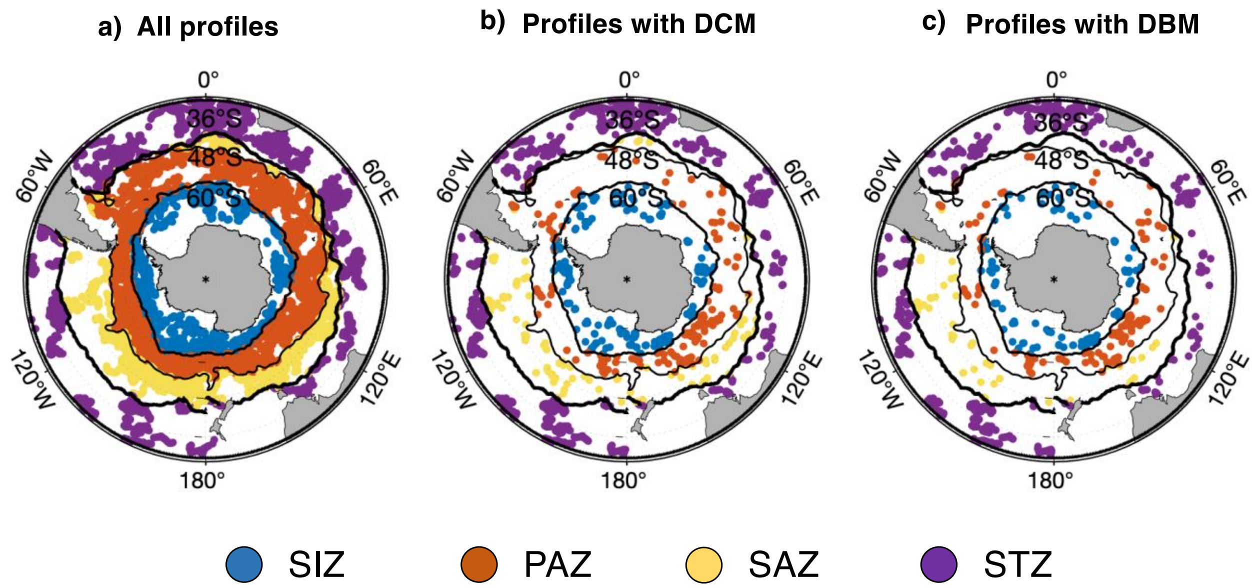


Figure 1. Location of (a) all 12,700 profiles used for the calculation of NPP, (b) 2,119 profiles with a DCM below the MLD, and (c) 1,363 profiles where a DCM was also a DBM. Colors represent the frontal zone in which each profile occurred as follows: sea ice zone (SIZ) south of the maximum sea-ice extent; polar Antarctic zone (PAZ) between the SIZ and polar Antarctic front; Subantarctic zone (SAZ) between the sub-Antarctic and sub-tropical front; subtropical zone (STZ) north of the sub-tropical front and south of 30°S. Fronts are based on Bushinsky et al. (2017) and the climatological maximum winter sea ice extent was computed using Copernicus Ocean and Sea Ice Satellite Application Facility (OSI SAF) products as per Liniger et al. (2024).

Float-based practical salinity and *in situ* temperature, adjusted and quality-controlled, were used to calculate absolute salinity, conservative temperature, and density using the Gibbs-Seawater Oceanographic Toolbox (McDougall & Baker, 2011, https://www.teos-10.org). The MLD was calculated based on a density difference of 0.03 kg $m^{-3}$ from density at 10m (de Boyer Montégut et al. 2004). The nitracline depth ($D_{NO3}$) was defined as the shallowest depth where the nitrate gradient exceeded 0.05 µmol kg $^{-1}$ m $^{-1}$ (Letelier et al. 2004) in a nitrate profile smoothed by a 10-point running median. This method for calculating $D_{NO3}$ is appropriate for HNLC areas, where nitrate tends to be more than 10 µmol kg $^{-1}$ at the surface (Arteaga et al. 2022).

### 2.1.1. Chlorophyll and phytoplankton carbon

During the routine BGC-Argo QC, the adjusted chl data are dark-corrected, NPQ (non-photochemical quenching)-corrected, and divided by 2, reflecting the global linear scaling factor between the factory calibration and *in situ* chlorophyll (Schmechtig et al. 2015; Boss and Haëntjens 2016; Roesler et al. 2017). The correction factor is larger in the SO due to iron limitation; we therefore multiplied chl by 2 (to remove the pre-applied correction) and applied an average slope factor for the Southern Ocean, dividing by 3.79 (Schallenberg et al. 2022). A 7-point running median filter was applied to both chl and $b_{bp}$ profiles as a despiking method (Su et al. 2021; Arteaga et al. 2022). This removed spikes due to measurement and background noise, and large phytoplankton aggregates (Briggs et al. 2011; Cornec et al. 2021). The mean value of chl in the mixed layer (ML) was defined as $chl_{MLD}$, and used to examine the relationship between subsurface NPP and the DCM in the correlation analyses.

We calculated $C_{phyto}$ based on $b_{bp}$ from the floats. First, to remove any non-phytoplankton signal, the mean $b_{bp}$ between 900 and 1000m was subtracted from the entire float profile (Arteaga et al. 2020). Next, $b_{bp}$ at 700nm, measured by the floats, was converted to $b_{bp}$ at 470nm, according to Morel and Maritorena (2001):

$$b_{bp470} = b_{bp700}\left(\frac{470}{700}\right)^{-1} \ \mathrm{m}^{-1} \tag{1}$$

Then, $C_{phyto}$ was estimated from $b_{bp470}$ using the empirical relationship from Graff et al. (2015):

$$C_{phyto} = 12{,}128\times b_{bp470} + 0.59 \ \mathrm{mg\ C\ m^{-3}} \tag{2}$$

This is based on a global analysis using backscatter and flow cytometry data from the field. This equation has been used in float-based estimates of NPP using $b_{bp}$ in the North Atlantic (Estapa et al. 2019, Yang et al. 2020), the Gulf of Mexico (Yang et al. 2022) and more recently in the SO (Arteaga et al. 2022).

## 2.2. Attenuation coefficient and euphotic depth

The diffuse attenuation coefficient at 490nm ($Kd_{490}$) was calculated for each depth using chl profiles from the floats (Morel et al., 2007):

$$Kd_{490}(z) = 0.0166 + 0.0773 \times chl(z)^{0.67155}\ m^{-1} \quad (3)$$

The satellite-derived surface photosynthetically available radiation ($PAR_{SURF}$) was obtained from NASA MODIS-Aqua (8-day, 9-km composites), downloaded from the NASA Ocean Color website (https://oceancolor.gsfc.nasa.gov). Each float profile was matched with a satellite value for $PAR_{SURF}$ (E $m^{-2}$ $day^{-1}$). The diffuse attenuation coefficient of PAR ($Kd_{PAR}$) was calculated for each depth using $Kd_{490}(z)$ and the MLD (Morel et al., 2007):

$$Kd_{PAR}(z) = 0.0864 + 0.884\ Kd_{490} - 0.00137 \times Kd_{490}^{-1}, \text{ when MLD} \leq Kd_{490}^{-1} \quad (4a)$$

$$Kd_{PAR}(z) = 0.0665 + 0.874\ Kd_{490} - 0.00121 \times Kd_{490}^{-1}, \text{ when MLD} > Kd_{490}^{-1} \quad (4b)$$

The profile of PAR, denoted PAR(z) was calculated using:

$$PAR(z) = PAR_{SURF} \times e^{(-Kd_{PAR}(z))} \quad (5)$$

The euphotic depth ($D_{eu}$) was defined as the depth where PAR(z) was 0.1% of $PAR_{SURF}$ (Laws et al., 2014).

## 2.3. Carbon-based Productivity Model (CbPM)

The model used in this study is the Carbon-based Productivity Model (CbPM; Behrenfeld et al. 2005; Westberry et al., 2008), which has been recently applied to *in situ* profiles of chl (mg chl $m^{-3}$) and $C_{phyto}$ (mg C $m^{-3}$) derived from BGC-Argo floats (Estapa et al. 2019, Long et al. 2021; Yang et al. 2021, 2022, Arteaga et al. 2022). The CbPM uses chl and phytoplankton carbon biomass ($C_{phyto}$) to estimate NPP.

The CbPM uses the chl:C ratio at each depth (z) as an indicator of phytoplankton nutrient (*g*) and light (*f*) stress, and to estimate the phytoplankton division rate (μ, $d^{-1}$). The cellular light index (*f*) is defined as:

$$f(z) = 1 - e^{(-5.0\ PAR(z))} \quad (6)$$

The CbPM assumes a well-mixed water column, homogeneous in the ML, and uses surface values from satellite as the mean value in the ML. We consider two scenarios for the mixed layer: a mixed and a stratified (depth-resolved) scenario. The mixed scenario uses the median PAR in the mixed layer ($PAR_{MLD}$) in place of PAR(z) in Eq. 6. Below the mixed layer, to 300m, PAR(z) is used. The depth-resolved scenario simply uses PAR(z) from the surface to 300m. Most profiles are aphotic below ~150m (Boyd et al. 2024), so $NPP_z$ from ~150 to 300m tends to be zero and contributes little to total integrated NPP (Figure 2d). We present the mixed scenario in the main manuscript with a brief mention of the depth-resolved scenario, and all figures from the latter in the SI.

The CbPM, as adapted by Westberry et al. 2008, derives chl:C ratios below the ML based on the phytoplankton response to light and nutrient limitation, and a theoretical chl:C maximum (chl:$C_{max}$), at each light level:

$$\text{chl:C}(z) = [0.022 + (0.045\text{-}0.022)\, e^{-3.0 \times \text{PAR}(z)}] - [\Delta\frac{chl}{C_{NUT}}\ (1 - e^{-0.075 Dz_{DNO3}}] \qquad (7)$$

Where $\Delta\frac{chl}{C_{NUT}}$ is the nutrient stress index ($g$), and is the difference between the surface chl:C and the chl:$C_{max}$:

$$\text{chl:C}_{max}(z) = 0.022 + (0.045 - 0.022) \times e^{-3.0\ \text{PAR}(z)/\text{daylength}} \qquad (8)$$

When light decreases, chl:C ratios increase as phytoplankton increase their cellular pigments to acclimate to low light (Geider et al. 1997; Graff et al. 2016). So chl:C ratios generally increase with depth due to photoacclimation. This trend is further affected by relaxation of nutrient stress, which is also depth-dependent. Nutrient stress increases with distance to the nitracline ($Dz_{DNO3}$), i.e., from depth towards the surface, and chl:C ratios decrease with nutrient stress. The chl:C ratio resulting from the light level at each depth and the distance to the nitracline (with the nitracline depth derived from climatologies) determines phytoplankton growth rates (μ) at each depth. The C biomass below the ML is then calculated based on growth and losses, defined by a constant growing rate (R = 0.1 $d^{-1}$).

Because we are using full profiles of chl and $b_{bp}$ from the floats, there is no need to reconstruct chl:C ratios below the ML based on a light or nutrient index. Instead, the cellular nutrient index ($g$), at each light level, was modelled following Arteaga et al. (2022), skipping Eq. 7 and using the float profiles directly in Eq. 9:

$$g\ (z) = \frac{\text{chl:C}(z) - \text{chl:C}_{\mu=0}}{\text{chl:C}_{max}(z) - \text{chl:C}_{\mu=0}} \qquad (9)$$

where chl:$C_{\mu=0}$ was set to 0.0003 mg chl mg $C^{-1}$, based on the minimum observed satellite chl:C (Westberry et al. 2008).

The phytoplankton growth rate (μ, $d^{-1}$) is then estimated at each depth (z) using the equation

$$\mu(z) = \mu_{max} \times g\ (z) \times f\ (z) \qquad (10)$$

where $\mu_{max}$ was set to 2, based on a natural observed maximum growth rate (Banse, 1991). Finally, the depth-resolved daily net primary production (NPP, mg C $m^{-3}$ $d^{-1}$) from the CbPM was computed using the $C_{phyto}$ derived from the $b_{bp}$ float profile as follows:

$$\mathrm{NPP}(z) = \mu(z) \times C_{phyto}(z) \quad (11)$$

### 2.4. Identifying deep chlorophyll and biomass maxima

To find "true" DCMs only, a 5-point running median was applied (Cornec et al. 2021) to an interpolated 300m profile of chl with a resolution of 1m, different from the smoothed profile used to estimate NPP, which is smoothed using a 7-point running median filter (section 2.1.1 in Methods). The $b_{bp}$ profile was smoothed with a 5-point running median followed by a 5-point running mean (Cornec et al., 2021). We defined the DCM as the depth of the maximum value of chl when that maximum value was deeper than 10m and the chl concentration at that depth was more than double the chl concentration in the upper 15m (Figure 2a; Lavigne et al., 2015; Cornec et al., 2021). The deep biomass maximum (DBM) is the depth of the maximum value of $b_{bp}$, when the $b_{bp}$ concentration at that depth is 1.3 times greater than the $b_{bp}$ concentration in the upper 15m (Cornec et al., 2021). In our 12,700 eligible NPP profiles (Figure 1a), we found a total of 2,306 DCMs following this criterion. For this study, we only consider DCMs below the MLD (2,119 out of 2,306 or 91%), as all other DCMs are expected to be spurious (Brown et al., 2015). Of these, 64% (i.e. 1,363) were also DBMs. We denote the depth of the DCM as $DCM_z$ and the depth of the DBM as $DBM_z$.

### 2.5. Subsurface production

The upper bound of the DCM ($DCM_{upper}$) was defined as the depth where the vertical chl gradient was the absolute maximum, above the $DCM_z$. Then the lower bound of the DCM ($DCM_{lower}$) was defined as $DCM_z$ + ($DCM_z$ – $DCM_{upper}$). Some DCMs were thinner (i.e., narrower depth range) than others, and therefore usually had a steeper chl gradient.

We define three measures of subsurface production. NPP integrated across the thickness of the DCM feature (15m average; $NPP_{DCM}$ Figure 2c) and the DBM feature (26m average; $NPP_{DBM}$ Figure 2a) was only estimated if a 'true' DCM or DBM was present. NPP below the MLD ($NPP_{SUB}$) was calculated as the integral of NPP below the MLD to 300m (Figure 2d). We use NPP "ALL" to denote all profiles with and without a DCM, and NPP "DCM" for profiles where a DCM was present below the MLD. Then, we calculate two types of percentages: (1) the contribution of $NPP_{DCM\ or\ DBM}$ to the total NPP when DCMs/DBMs are present, and (2) the contribution of $NPP_{SUB}$ to the total NPP when DCMs/DBMs are present or not (Table 1). For profiles that had a DCM/DBM, we removed the DCM/DBM and recalculated NPP, to understand the significance of the DCM/DBM. We removed the DCM/DBM as follows: below the MLD, we take the BGC-Argo measured chl or $b_{bp}$ value at each depth if it is smaller than the median MLD value. Otherwise, we take the median MLD value. We then apply the CbPM the same way we did with the original Argo float profiles. All estimates from this method are denoted $NPP_{DCM\text{-}removed}$ and $NPP_{DBM\text{-}removed}$ (see Figure 2 for examples).

### 2.6. NPP estimates from satellite

To compare our BGC-Argo NPP estimates to satellite estimates, we derived NPP below the ML using all the same assumptions as are used for the satellite application of the CbPM, but using the float median in the ML as the surface value instead of the satellite value (Arteaga et al., 2022). In the adapted CbPM by Westberry et al. (2008), the cellular nutrient index (*g*) uses the distance to the nitracline at each depth (Eq. 7-9). Recently, Arteaga et al. (2022) showed that changing the nitracline depth for the ferricline depth south of 30°S improved the NPP estimates from satellite. Here, we use the CbPM (nitracline) adapted by Westberry et al. (2008), using nitracline depths computed using nitrate profiles from the floats, (NPP $Sat_{nit}$), and the CbPM (ferricline) adapted by Arteaga et al. (2022), using a mean ferricline of 333m depth (NPP $Sat_{fer}$), based on in situ estimates in the Southern Ocean from Tagliabue et al. (2014).

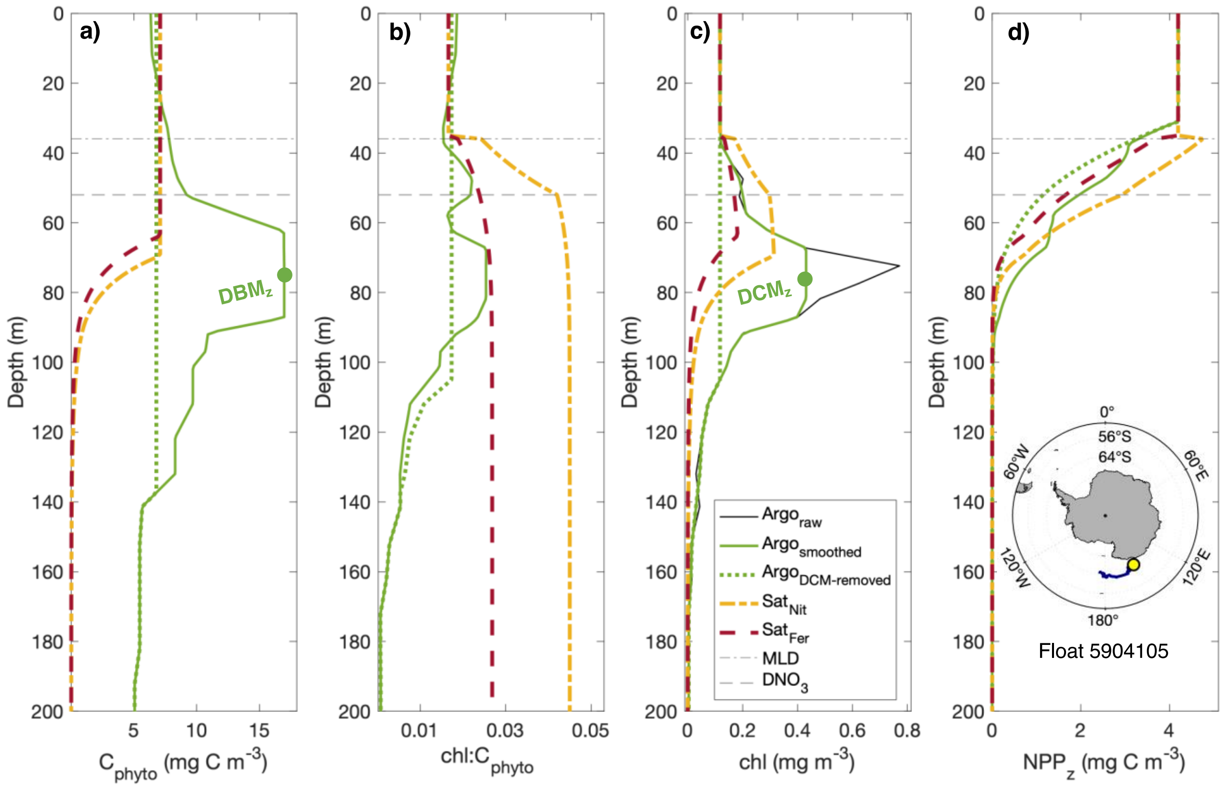


Figure 2. Profiles of (a) $C_{phyto}$, (b) chl:$C_{phyto}$ ratio, (c) chl, and d) NPP resulting from the range of methods. Note that in this figure, all profiles are only shown to 200m as NPP below 200m was zero. The black line in panel c) represents the chl profile after applying all quality control criteria and before smoothing, used to calculate NPP. The solid green line is the smoothed profile from the float. The dashed green is for the float profile after removing the DCM. The dashed yellow line is for the CbPM using the nitracline and the dashed red line is for the CbPM using the ferricline to calculate the nutrient index. In all four panels, the same profile (no. 4) from float WMO5904105 is shown. Both, the MLD and the nitracline depth for this profile are shown in all panels. The ferricline depth in the $CbPM_{Fer}$ was set to 333m in all profiles (Arteaga et al. 2022).

All NPP estimates (Table 1) were not normally distributed, therefore the Kruskal-Wallis test was used to test for significant differences between variables across DCM, DBM, and ALL. To test differences in subsurface NPP between zones, the Kruskal-Wallis and Dunn's post-hoc tests were used. A correlation test was used to examine the influence of environmental variables ($PAR_{MLD}$, $D_{NO3}$, $DCM_z$, $DBM_z$, MLD, $D_{eu}$, and $chl_{MLD}$) on the contribution of subsurface production to total production from the different profiles. Root mean square error, mean normalised bias, and the correlation coefficient (r), were used to compare NPP estimates between the $CbPM_{Nit}$, $CbPM_{Fer}$, $Argo_{DCM\text{-}removed}$ and Argo float profiles. All analyses, including statistical analyses, were carried out using MATLAB ver. R2018b.

Table 1. Definitions of the acronyms used to describe the different (subsurface) production measures.

| Label | Definition |
|---|---|
| NPP (ALL) | Vertically-integrated NPP for all profiles, with and without a DCM |
| NPP (DCM) | Vertically-integrated NPP for profiles with a DCM |
| NPP (DBM) | Vertically-integrated NPP for profiles with a DBM |
| $NPP_{DCM\text{-}removed}$ | Vertically-integrated NPP for profiles with a DCM, after removing the DCM |
| $NPP_{DBM\text{-}removed}$ | Vertically-integrated NPP for profiles with a DCM, after removing the DBM |
| NPP $Sat_{nit}$ | Vertically-integrated NPP derived from surface values using the nitracline |
| NPP $Sat_{fer}$ | Vertically-integrated NPP derived from surface values using the ferricline |
| $NPP_{DCM}$ | Integrated NPP in the DCM |
| $NPP_{DBM}$ | Integrated NPP in the DBM |
| $NPP_{SUB}$ (DCM) | Integrated NPP below the MLD, for profiles with a DCM |
| $NPP_{SUB}$ (DBM) | Integrated NPP below the MLD, for profiles with a DBM |
| $NPP_{SUB}$ (ALL) | Integrated NPP below the MLD, for profiles with and without a DCM |
| $\%NPP_{DCM}$ | Percentage of NPP in DCM relative to total NPP |
| $\%NPP_{DBM}$ | Percentage of NPP in DBM relative to total NPP |
| $\%NPP_{SUB}$ (DCM) | Percentage of NPP below MLD relative to total NPP in profiles with a DCM |
| $\%NPP_{SUB}$ (DBM) | Percentage of NPP below MLD relative to total NPP in profiles with a DBM |
| $\%NPP_{SUB}$ (ALL) | Percentage of NPP below MLD relative to total NPP in all profiles |

## 3. Results

### 3.1. Deep chlorophyll maxima occur across the Southern Ocean and often coincide with deep biomass maxima

We observed a total of 2,133 DCMs in BGC-Argo float data from 30°S to Antarctica (Figure 1b). DCMs occur across the four frontal zones defined in this study (see Methods 2.1.), consistently throughout the year, with higher frequency in summer (Figure 4). DCMs are dominant in the STZ, with a total of 1,558 DCMs. South of the STZ, the SIZ had 255 DCMs, the PAZ 189 and the SAZ 131. North of 40°S, in the STZ, DCMs occur throughout the year. At 40-60°S DCMs are restricted to spring and summer (November to March), and south of 60°S DCMs occur from September to April (Figure 3). Notably, 63% of the DCMs occurring south of 30°S coincided with a DBM. By region, this amounted to 1,032 (75%) of DBMs in the STZ, 148 in the PAZ, 112 in the SIZ, and 67 in the SAZ. DCMs and DBMs most commonly occur deeper than 100m, and there is a tendency for concurrent DCMs to be found deeper than DBMs (Figure 5h). The widespread occurrence of DCMs and DBMs strongly suggests that they are ecologically important in the Southern Ocean, south of 30°S.

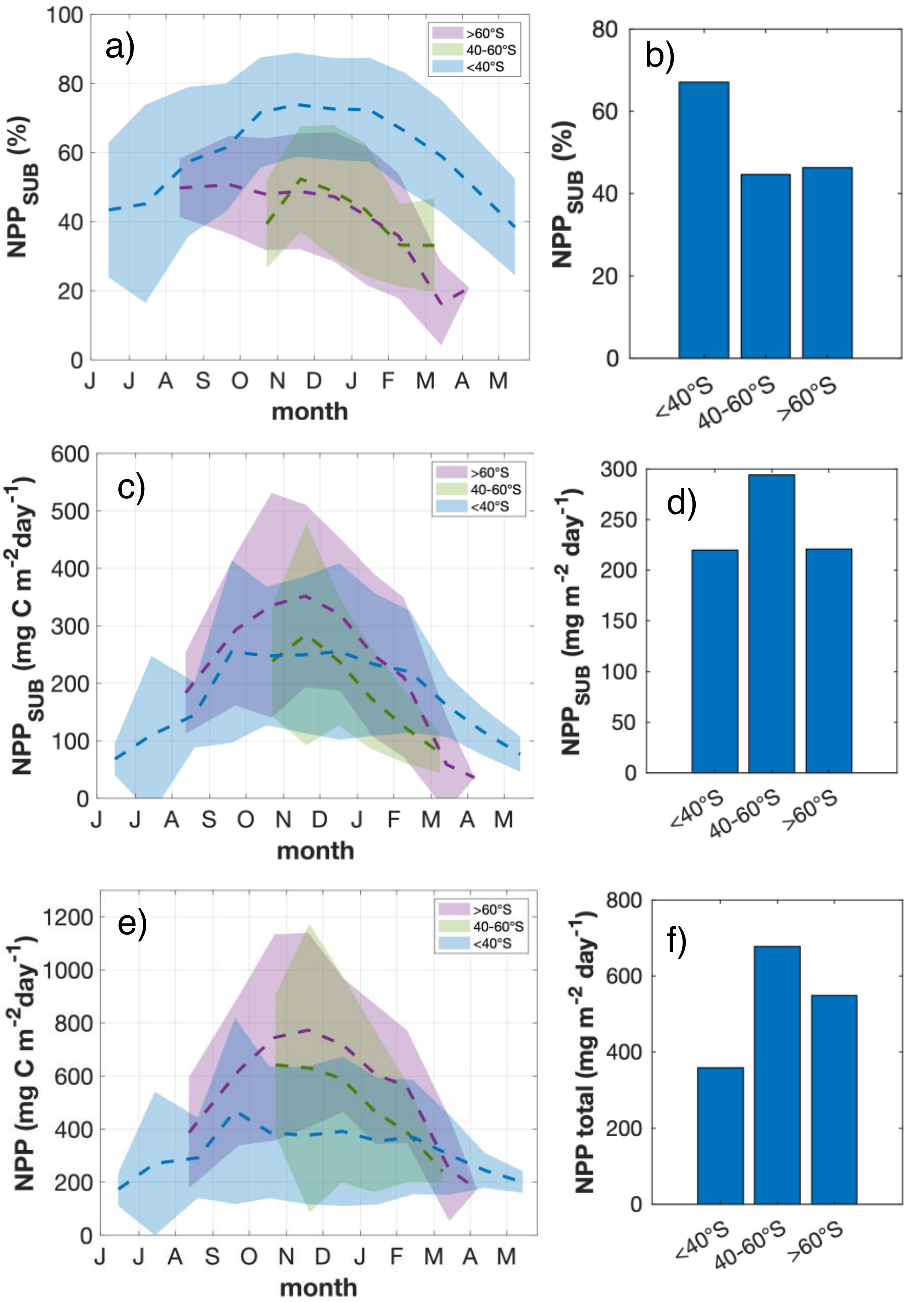


Figure 3. Seasonal cycles with monthly means (panels a, c and e) and annual means (panels b, d and f) for each latitudinal group: <40°S, 40-60°S, and >60°S. The contribution of subsurface NPP to total NPP is shown in panels a) and b), integrated subsurface NPP is shown in panels c) and d), and total integrated NPP in panels e) and f). The shorter timeseries in a, c and e are due to lack of DCM profiles outside of the summer and spring months at higher latitudes. Because there is no data from DCM profiles after summer, the contribution of subsurface NPP to total NPP decreases to 20%, although in winter, having no DCMs, the contribution will be zero.

## 3.2. How productive are deep chlorophyll maxima?

### 3.2.1. Total NPP estimates

Estimates of total integrated NPP (ALL) range from <100 to 1,500 mg C $m^{-2}$ $day^{-1}$ (Figure 4a) with a mean of 355 ± 396 mg C $m^{-2}$ $day^{-1}$ (standard deviation). Total production was on average higher when DCMs were present (Figure 5g). That is, mean NPP (DCM) (406 ± 306 mg C $m^{-2}$ $day^{-1}$) was significantly higher than mean NPP (ALL). Mean NPP (DBM) was lower (306 ± 248 mg C $m^{-2}$ $day^{-1}$) than mean NPP (ALL). Production was highest from November to January for these three parameters (Figure 4b). Summer is also the period when DCM occurrence was highest (Figure 4d). Total NPP increases in summer for profiles with and without DCMs or DBMs, but again, the overall seasonality is muted when DCMs or DBMs are present (Figure 4b). For NPP (ALL), on average, mid-latitudes (45-60°S) are more productive than the region impacted by sea-ice (>65°S; Figure 4c), where DCMs are less common (Figure 1b, 6b). The sea ice zone is impacted by ice cover, making it an annually low but seasonally highly productive area. NPP estimates are higher, although not significantly, when using the mixed scenario compared to the depth-resolved scenario (see Methods, 2.3.), but trends are similar (Table S3).

Our NPP estimates agree with in-situ measurements of NPP from previous studies in the Southern Ocean S of 30S (Figure 4c). The majority of in-situ measurements were taken during the austral spring and summer, when NPP is highest. Because our NPP and $NPP_{SUB}$ estimates depend heavily on accurate MLD calculations, we compare our MLD values with the literature (see SI.1.). The observed distribution of MLDs (Figure 6a; Figure S1-S4) is consistent with other studies using the density method (Table S1).

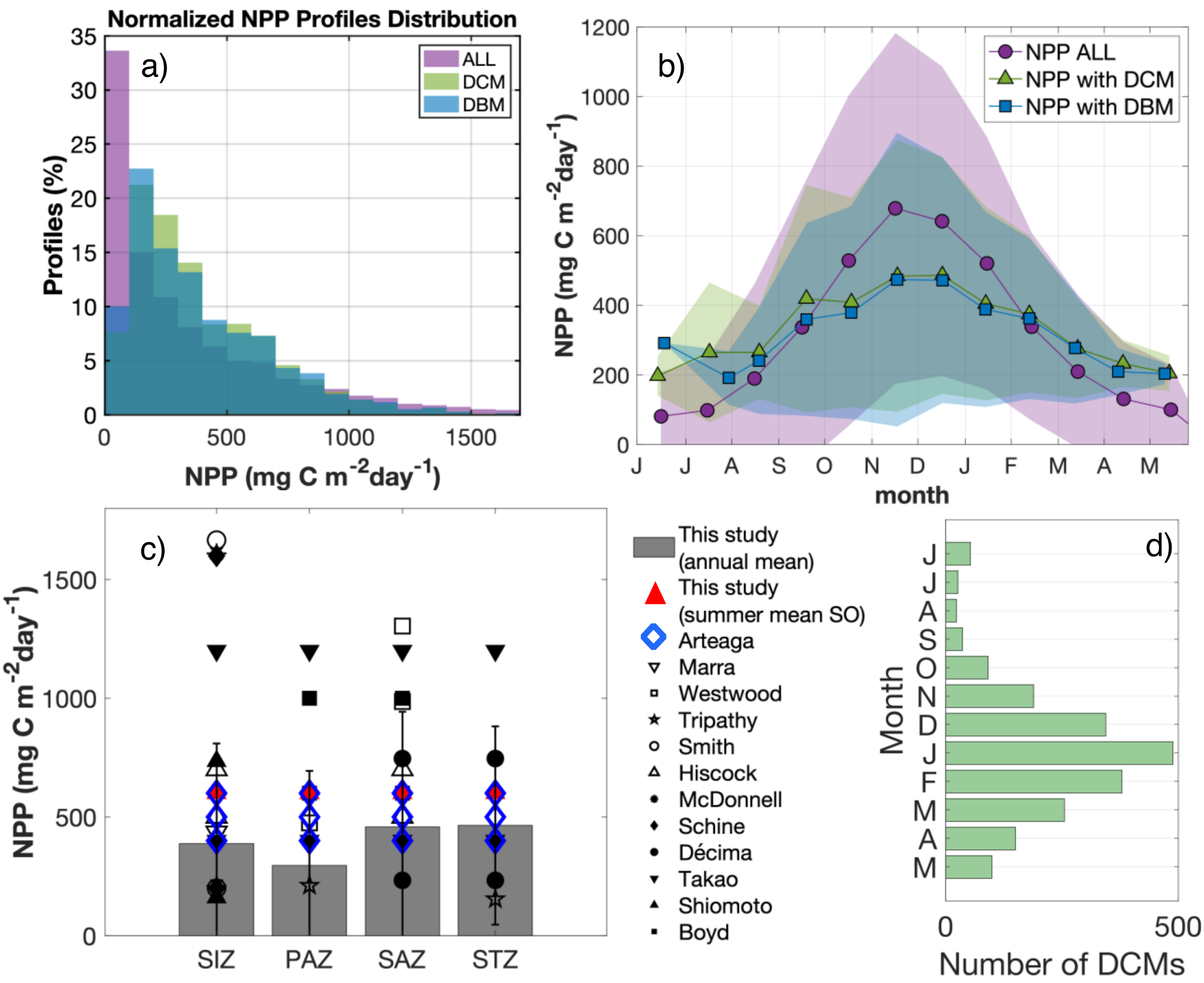


Figure 4. (a) Data distribution of total integrated NPP for all profiles (purple), profiles with a DCM (green), and profiles with a DBM (blue) shown as % of all profiles of each type. (b) The seasonal cycles with monthly means for total integrated NPP for the three data sets: ALL (purple), with a DCM (green), and with a DBM (blue). (c) Annual means of NPP (bars) and standard deviation (error bars) for each frontal zone in the Southern Ocean south of 30S, compared to total NPP estimates from other studies. The grey bars and red filled triangles correspond to our annual means for each frontal zone and summer mean for all data across the Southern Ocean, respectively. The Arteaga NPP estimates are based on BGC-Argo float profiles following the same methods as in this study. Because no annual means or overall means are reported in their study, we take estimates based on their Figure 9, where NPP estimates range from <100 to >800 mg C $m^{-2}$ $day^{-1}$ annually, and can reach 2000 mg C $m^{-2}$ $day^{-1}$, agreeing with our estimates. Other estimates are from mostly summer $^{14}C$ incubations. The DCM occurrence for each month is shown in panel d).

### 3.2.2. Deep chlorophyll and biomass maxima increase the contribution of subsurface NPP to total NPP

Profiles with a DCM and a DBM had significantly higher NPP below the mixed layer compared to all profiles together, with and without DCMs/DBMs (Figure 5; Table S2). $NPP_{SUB}$(DCM) and $NPP_{SUB}$(DBM) were 153 ± 108 and 161 ± 113 mg C $m^{-2}$ $day^{-1}$ respectively and $NPP_{SUB}$ for all profiles combined, $NPP_{SUB}$(ALL), was 21 ±103 mg C $m^{-2}$ $day^{-1}$; Table S2). Profiles with a DBM had significantly higher $NPP_{SUB}$(DBM) than profiles with a DCM only ($NPP_{SUB}$(DCM); Kruskal-Wallis $p<0.05$; Figure 5c). Similarly, $NPP_{DBM}$ was higher than $NPP_{DCM}$ (Figure 5b), but not significantly (86 ±124 vs. 57 ±118 mg C $m^{-2}$ $day^{-1}$, $p>0.05$).

When DCMs and DBMs are present, % $NPP_{SUB}$ increases significantly, compared to %$NPP_{SUB}$ in all profiles with and without DCMs and DBMs (76% median vs 1% median; Kruskal-Wallis $p<0.05$; Figure 5d). The contribution of NPP at the DCM to the total NPP in profiles where a DCM is present (%$NPP_{DCM}$) ranges between 40 and ~60% (median 26 ±12%; Figure 5d). NPP at the DBM contributes between 60 and ~80% with a median of 44±42% (%$NPP_{DBM}$, Figure 5d). The contribution of %$NPP_{DCM}$ is overall skewed towards lower values compared to %$NPP_{DBM}$, where the distribution of the data is constant across a wide range of values (Figure 5e). The distributions of %$NPP_{SUB}$(DCM) and %$NPP_{SUB}$(DBM) are skewed towards higher values, and %$NPP_{SUB}$(ALL) is skewed towards lower values (Figure 5f). Similar to the total NPP numbers, these conclusions are true for $NPP_{SUB}$ and %$NPP_{SUB}$ for both the mixed and the depth-resolved scenario (Table S3).

Because our $NPP_{SUB}$ estimates depend heavily on accurate MLD calculations, we compare our MLD values with the literature. The observed distribution of MLDs (Figure S2) is consistent with other studies using the density method (Table S1). An extended summary of this comparison can be found in section SI.1. in the SI.

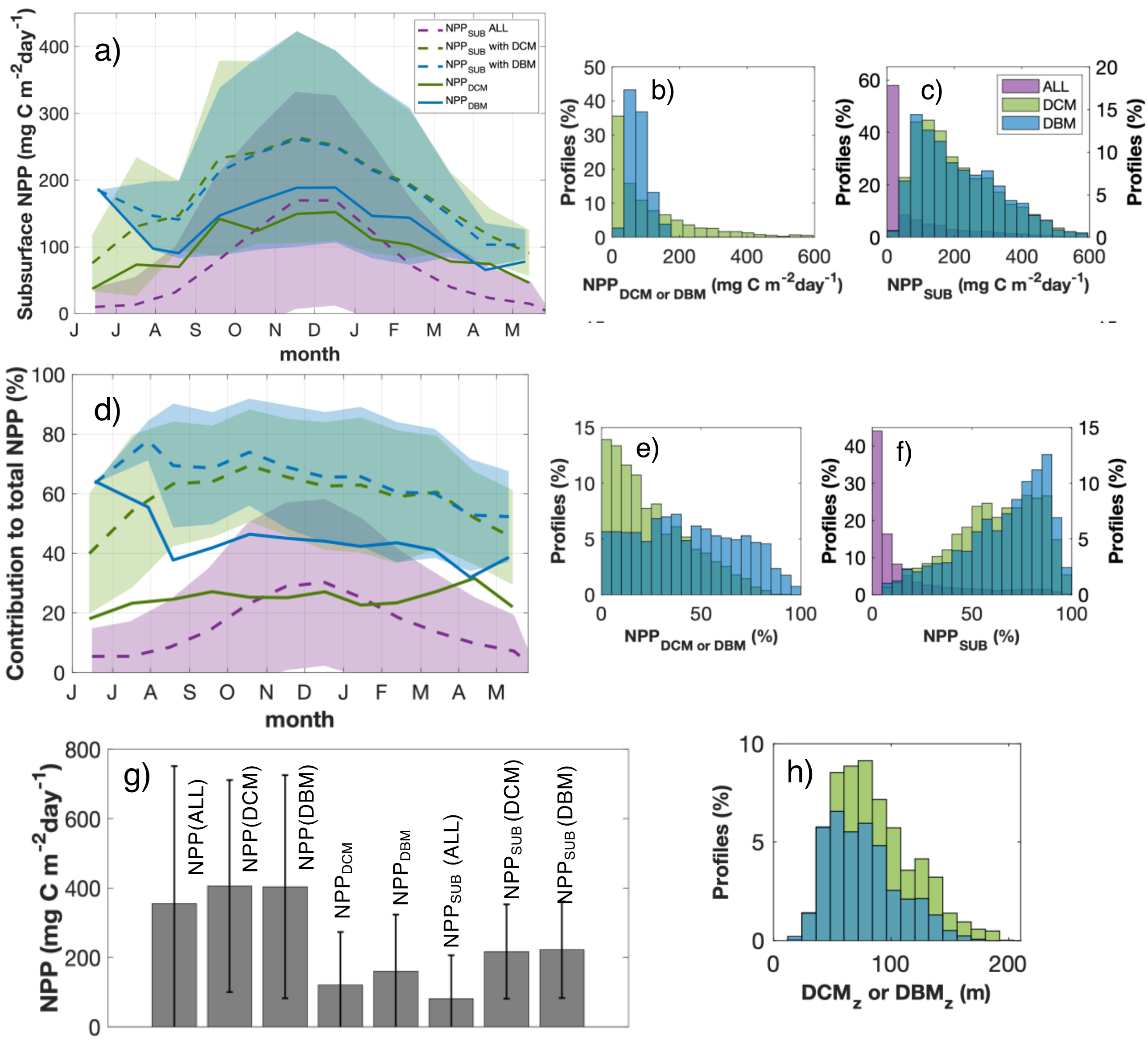


Figure 5. a) Seasonal distribution of subsurface NPP (mg C $m^{-2}$ $day^{-1}$) with monthly means and standard error for all profiles analysed (dashed purple line), profiles with a DCM (dashed green line), profiles with a DBM (dashed blue line), and NPP in the DCM layer (solid green line) and NPP in the DBM layer (solid blue line). b) Data distributions for NPP in the DCM layer (mg C $m^{-2}$ $day^{-1}$) and NPP in the DBM layer. c) Data distributions for subsurface NPP (mg C $m^{-2}$ $day^{-1}$) in all profiles, profiles with a DCM and profiles with a DBM. (d) Monthly means and standard error for the contribution of subsurface NPP to total NPP (%) for the same datasets as in panel a). Panels e) shows the distribution of $\%NPP_{DCM}$ and $\%NPP_{DBM}$, and (f) for $\%NPP_{SUB}$(DCM), $\%NPP_{SUB}$(DBM), and $\%NPP_{SUB}$(ALL). The right-hand axis in panels c) and f) corresponds to $NPP_{SUB}$(DCM), and $NPP_{SUB}$(DBM). Panel (g) shows means

and standard errors for all the NPP estimates including NPP in the DCM/DBM layer and subsurface NPP. The distribution of DCM and DBM depths is shown in panel h).

**3.3. Seasonal and spatial variability of production in DCMs and DBMs**

Subsurface NPP is strongly seasonal for all cases, but the difference between summer and winter is less stark when DCMs or DBMs are present (Figure 5a). $NPP_{SUB}$ ALL ranges from ~10 mg C $m^{-2}$ $day^{-1}$ in winter to 150 mg C $m^{-2}$ $day^{-1}$ in summer. $NPP_{SUB}$(DCM) increases from 100 mg C $m^{-2}$ $day^{-1}$ in winter to ~210 mg C $m^{-2}$ $day^{-1}$ in summer (Figure 5a), and the pattern for DBMs is very similar. $NPP_{SUB}$ (DCM/DBM) contributes to more than half of the total production consistently through the year, on average for all profiles with a DCM (Figure 5d). While %$NPP_{SUB}$(ALL) shows pronounced seasonality, %$NPP_{DCM}$ and %$NPP_{DBM}$ stay almost constant throughout the annual cycle at ~20% and ~45% respectively. At low latitudes (30-40°S), %$NPP_{SUB}$ is at least 40% throughout the year, and more than 50% during the summer. At mid latitudes (40-60°S), DCMs occur only in the summer and %$NPP_{SUB}$ decreases from 40 to 30% (Figure 3a and b). At high latitudes (>60°S), DCM occurrence extends over the spring and summer months, where %$NPP_{SUB}$ is ~40% during spring and then drops to <20% at the end of the summer.

Overall, the contribution of $NPP_{SUB}$ to NPP when DCMs are present is highest in subtropical oligotrophic regions of the Southern Ocean (30-40°S, Figure 3), compared to the iron and/or silicate-limited regions (40-60°S) and the iron-limited sea ice zone (>60°S). $NPP_{SUB}$ is highest at mid-latitudes (40-60°S), although these regions are the most productive overall, resulting in low %$NPP_{SUB.}$ DCMs are less important in regions of higher NPP, south of 40°S.

The seasonal patterns observed are likely related to the spatial patterns, which show that subsurface production is highest at lower latitudes (Figure 6, 7), where seasonality is weakest (Figure 5a). Across zones, %$NPP_{SUB}$ is much higher when DCMs (69 ± 20 %) and DBMs (75 ± 21 %) occur compared to all profiles, with and without DCMs (21 ± 25%; Table S2; Kruskal-Wallis $p<0.05$). However, the contribution of subsurface NPP to total NPP (%$NPP_{SUB}$) exhibits a different pattern. The lowest contribution is in the PAZ, which then increases towards the north, reaching a maximum at the STZ (Figure 6f; Figure 7). For all profiles, with and without a DCM, %$NPP_{SUB}$(ALL) reaches a maximum of approximately 40% in the STZ, with much lower values observed at higher latitudes (Figure 7). Moreover,

%$NPP_{SUB}$(DCM) and (DBM) reaches up to 70% north of the sub-tropical front and decreases towards higher latitudes, until it increases again somewhat near Antarctica (Figure 6f; 7a). Indeed, the contribution of subsurface NPP to total NPP is always highest in the STZ (Dunn's test, $p<0.0$; Figure 7; Table S2). Overall, both, subsurface NPP and its contribution to total NPP, are higher in the northern zones. That is, contribution of $NPP_{SUB}$(DCM) and $NPP_{SUB}$(DBM) to total NPP is highest in less productive areas or times (Figure 4b), for example in the summer and at low latitudes, where DCMs and DBMs occur.

In contrast, the amount of NPP below the MLD, and its contribution to total NPP, is lower in areas with more production and fewer DCM and DBM occurrence. In regions characterized by overall lower NPP (Figure 6c), such as the Pacific and Atlantic sections of the Subtropical Zone (STZ), we find more subsurface production (Figure 6e,f), particularly in areas with deeper DCMs and DBMs (Figure 6b), and lower surface nitrate (Figure 6d). Thus, the influence of DCMs on the contribution of subsurface NPP increases when total NPP decreases. These general trends are true for both the mixed and the depth-resolved scenario, where $NPP_{SUB}$ is generally higher when DCMs and DBMs are present (Table S3).

We find no significant correlations with surface $NO_3$, and we find that DCMs and DBMs occur, even when surface $NO_3$ is high, indicating iron limitation in HNLC areas in the Southern Ocean (Figures S6-S11). Not surprisingly, we find positive correlations between $NPP_{SUB}$ (ALL, DCM and DBM) and light ($PAR_{MLD}$ only, not $D_{eu}$), but these are significant only in the PAZ (Table S4). See SI for additional figures and results (Figures S6-S11; Tables S4 and S5). We find that DCMs occur across the Southern Ocean, where light and iron are limiting. The %$NPP_{SUB}$ is higher at low latitudes, where DCMs are deeper and total NPP is low (Figure 6).

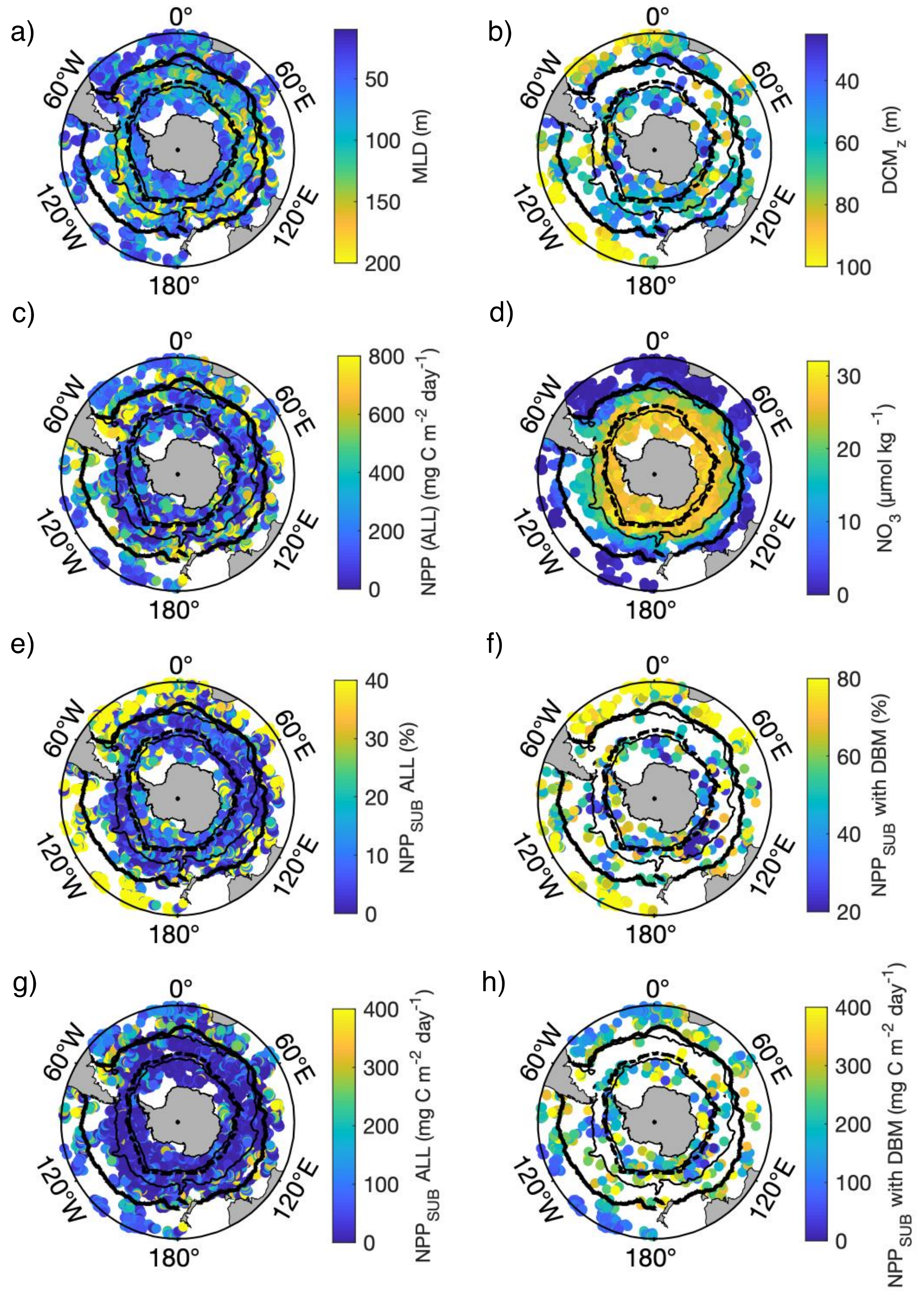


Figure 6. Spatial distribution of (a) MLD for all profiles with and without a DCM, (b) DCM depth ($DCM_z$) (c) total integrated NPP for all float profiles, (d) surface nitrate averaged over the upper 20m (e) the contribution of $NPP_{SUB}$ to total NPP (%) for all float profiles, (f) the contribution of $NPP_{SUB}$ to total NPP (%) when a DCM and DBM is present, (g) below-

mixed-layer NPP for all float profiles (mg C m$^{-2}$ day$^{-1}$), and (h) below-mixed-layer NPP in the presence of a DCM and a DBM (mg C m$^{-2}$ day$^{-1}$). The black lines represent the polar front, the sub-Antarctic front, and the sub-tropical front. The dashed black line shows the limit of the sea-ice zone.

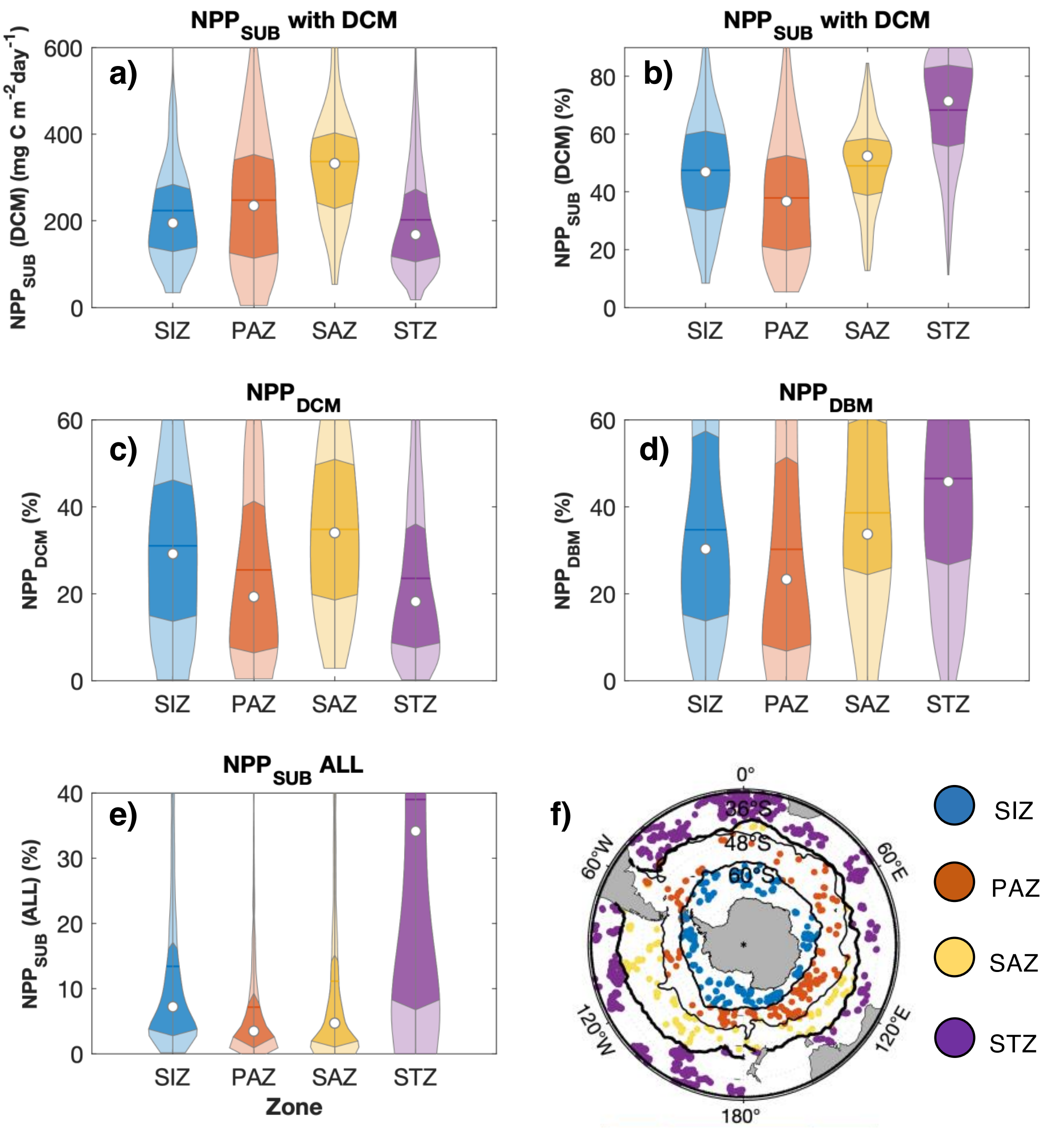


Figure 7. Violin plots for the four frontal zones, showing: (a) NPP below the MLD when DCMs occur (mg C m$^{-2}$ day$^{-1}$), (b) the contribution to total NPP from NPP below the MLD expressed as a percentage, (c) the contribution of NPP at the DCM to total NPP (%), (d) the contribution of NPP at the DBM to total NPP (%), (e) the contribution of NPP below the MLD to total NPP (%) for all profiles with and without DCMs and DBMs. The shaded area shows the distribution of data for each group, the darker shade is the interquartile range, the coloured horizontal line is the mean value, and the white circle is the median value. Panel (f)

shows all the float profiles with a DCM in each frontal zone. The extended version of this figure is presented in figure S5; it includes all $NPP_{SUB}$ estimates, and their contributions to total NPP, for all frontal zones.

### 3.4. How do satellites represent NPP associated with DCMs and DBMs?

The CbPM satellite algorithm doesn't explicitly account for DCMs or DBMs, but it does use the chl:C carbon ratio to mimic what happens below the ML. In order to investigate how well it does when DCMs/DBMs are present, we compare our Argo-derived NPP estimates to estimates that use the same assumptions as the satellite algorithms, but with mixed-layer chl and carbon estimates from the Argo floats, so that results are directly comparable ($NPP_{SAT}$; see Methods section 2.6). Overall, the CbPM overestimates NPP across the Southern Ocean when using the nitracline to estimate the nutrient index (Figure 8a, Figure 9a,b), as found previously by Arteaga et al. (2022). Overestimates are highest in the low and high latitudes, and smallest in the mid-latitudes (Figure S12). The CbPM performance improves when the mean depth of the ferricline is used as a nutrient reference instead of the nitracline, bringing NPP estimates closer to the float estimates (Figure 9c,d). Again, however, the discrepancies are highest at the high and low latitudes (Figure 8a). Interestingly, when comparing only profiles where a DCM was present, NPP $Sat_{Fer}$ compares very favourably to the float estimates, even better than when all profiles are compared (compare Figure 8a and b, 9c,d). The ferricline version performs best when DCMs are present (r=0.88, RMSE=378.8, P-bias=42.18), compared to all profiles with and without a DCM (r=0.70, RMSE=398.3, P-bias=52.85).

Inspecting the NPP estimates for the subsurface (Figure 8c and d), we find that the satellite algorithm "creates" a DCM (both for the ferricline and nitracline parameterization; Figure S13 in the SI). Even though this feature does not usually sit at the same depth as the measured DCM, it nudges the satellite algorithm towards higher column-integrated NPP for cases where a DCM is present, hence the better agreement with the observations. The nitracline parameterization overestimates NPP for all cases (Figure 9a and b). The ferricline parameterization, however, does well for DCM cases and somewhat over-estimates NPP when no DCM is present (Figure 9c and d).

Our results show that when we remove the DCM from the float profile, average estimates are 139 mg C $m^{-2}$ $day^{-1}$ and thus 34-45% (mean and median) lower than the total NPP with DCM. When the DBM is removed, these numbers are 49.13-88.5 mg C $m^{-2}$ $day^{-1}$ (mean and median) and 16-37% lower of the total NPP.

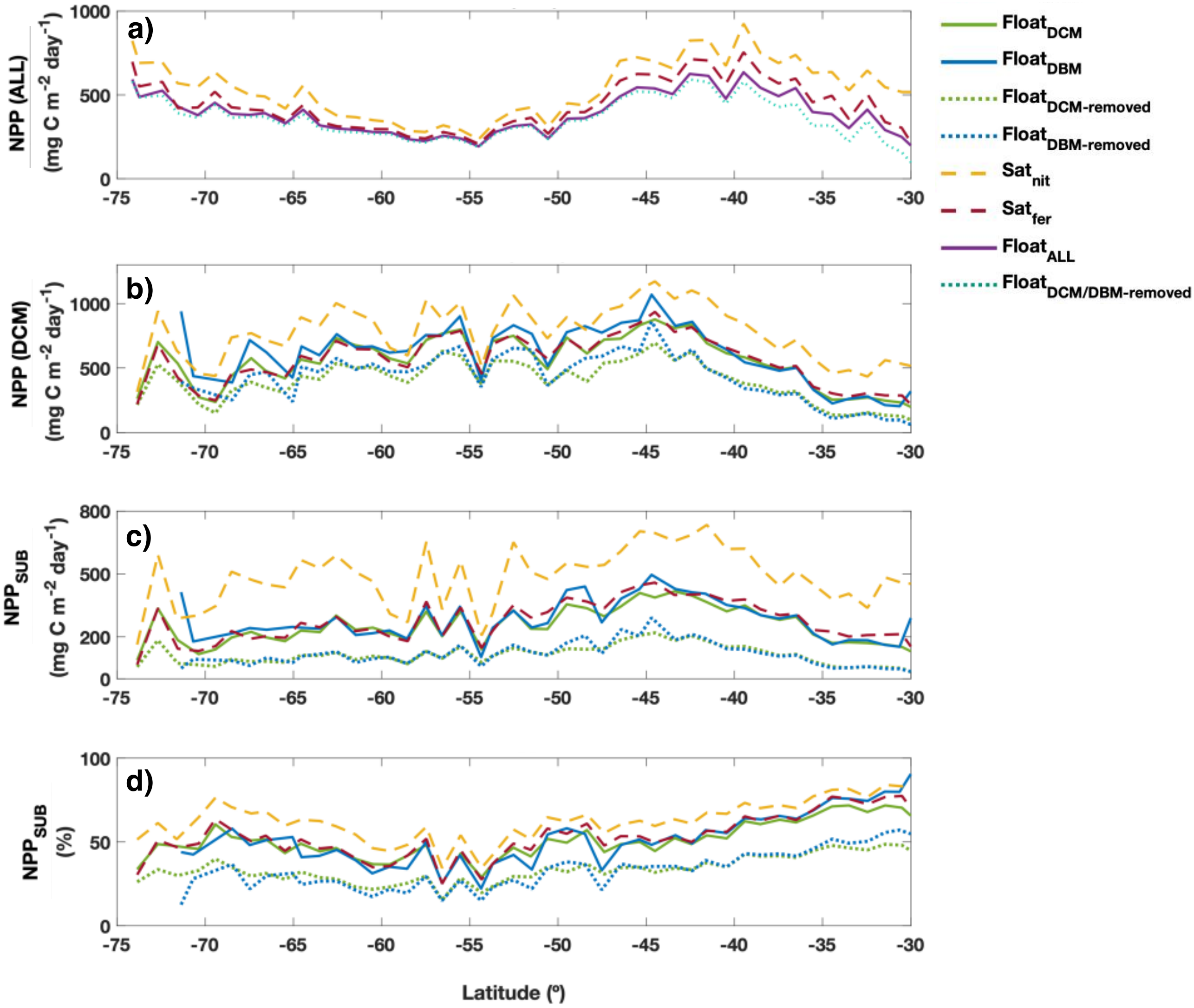


Figure 8. Latitudinal mean values for (a) total NPP (mg C $m^{-2}$ $day^{-1}$) in all the profiles, with and without a DCM present, (b) total NPP (mg C $m^{-2}$ $day^{-1}$) in profiles with a DCM present, (c) $NPP_{SUB}$ (mg C $m^{-2}$ $day^{-1}$) for profiles with a DCM, and (d) $NPP_{SUB}$ as a percentage (%) of total NPP in profiles where a DCM was present. The estimates are shown for all four methods: using the Argo float profiles of chl and carbon, in profiles with a DCM (solid green) and profiles with a DBM (solid blue), artificially removing the DCM from the same

float profile (dashed green) and removing the DBM (dashed blue), using the CbPM with the nitracline (dashed yellow) and the CbPM with the ferricline (dashed red).

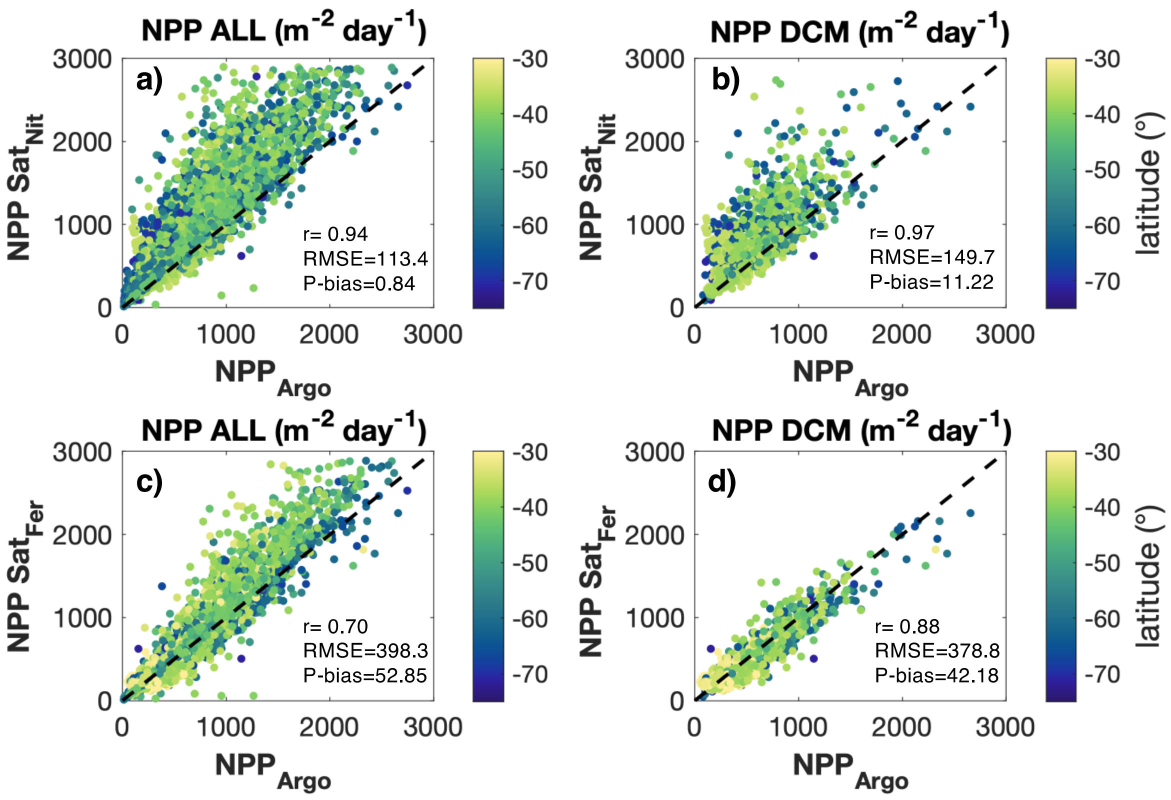


Figure 9. Scatterplots of vertically-integrated NPP a) from satellite estimates using the Carbon-based Productivity Model (CbPM) with the nitracline compared to Argo profiles with and without a DCM, and b) in profiles where a DCM is present, c) from satellite estimates using the CbPM with the ferricline compared to Argo profiles with and without a DCM, and d) in profiles where a DCM is present. The correlation coefficient (r) is shown on each panel, along with the root mean square error (RMSE, mg C $m^{-2}$ $day^{-1}$) and the mean normalised bias (P-bias, mg C $m^{-2}$ $day^{-1}$).

## 4. Discussion

### 4.1. DCMs are prevalent across the Southern Ocean

The latitudinal pattern we observed, namely more common DCMs and DBMs towards the north, ~30 to 50°S, is likely linked to the similar gradient in water-column stability, nutrients and light, following the standard DCM conceptual model at low latitudes (Cullen, 2015). Stratified, two-layer conditions are commonly perceived as essential for the formation of DCMs (Cullen, 2015; Latasa et al., 2017). This stratification is observed less often towards the poles and in winter in the Southern Ocean (Cornec et al., 2021). At the same time, the magnitude of the seasonal variability in the ML decreases towards low latitudes. Previous studies have also observed an increase in DCM occurrence from the poles to the equator (Parslow et al., 2001; Ardyna et al., 2013; Mignot et al., 2014; Cullen, 2015; Silsbe and Malkin, 2016; Baldry et al., 2020; Cornec et al 2021).

Recent research has revealed DCMs in the Southern Ocean using BGC-Argo float profiles (Pinkerton et al., 2021; Cornec et al., 2021; Yasunaka et al., 2022; Strutton et al., 2023), as well as ship-based measurements (Carranza et al., 2018; Latour et al., 2023; Boyd et al., 2024). While our understanding of DCMs largely stems from nitrate-limited waters (Cullen 2015), various mechanisms regarding their formation have been observed for the iron-limited Southern Ocean. These include photoacclimation (Baldry et al., 2020; Cornec et al., 2021a), physical or biogeochemical mechanisms such as eddies (Cornec et al., 2021b; Strutton et al., 2023), sea-ice retreat, subduction, and episodic iron supplies that induce diatom aggregations at depth (Carranza et al., 2018; Baldry et al., 2020). More recently, persistent DCMs and DBMs have been found near a subsurface ammonium maximum, suggesting a sustained in situ supply of recycled iron along with silicate resupply from depth (Boyd et al., 2024). The higher prevalence of DCMs at the STZ, and in the SIZ during summer, where light is less limiting, and their strong association with DBMs, confirm that mechanisms other than photo-acclimation contribute to their formation in the Southern Ocean, agreeing with mechanisms documented in temperate and tropical waters (Durham and Stocker, 2012).

### 4.2. Deep chlorophyll maxima matter for Southern Ocean primary production

We observe DCMs and DBMs everywhere in the Southern Ocean, and while we do see higher abundance at low latitudes in the STZ, compared to the PAZ and SAZ, DCMs and DBMs are widespread, and occur under a range of light and nutrient conditions. More importantly, our results show that DCMs are significant in terms of their contribution to total production. Subsurface NPP in the presence of DCMs contributes 59% of total NPP on average. This contribution is highest (40-70%) north of 40°S, and lower (20-40%) south of 40°S (Figure 3). At low latitudes, the contribution of DCMs is consistent throughout the year, while in iron-limited areas south of 40 and 60°S the contribution shows strong seasonality, lasting a few months during spring and summer, where the contribution decreases to ~20% towards the end of the summer. When DCMs and DBMs are present, $\%NPP_{SUB}$ increases significantly, compared to $\%NPP_{SUB}$ in all profiles with and without DCMs and DBMs (76% median vs 1% median). When DCMs are not accounted for or removed, NPP is 34-45% lower than total NPP from profiles with a DCM.

While DCM studies are limited in the Southern Ocean compared to other basins, previous Southern Ocean work found higher productivity (211 vs. 152 mg C $m^{-2}$ $day^{-1}$) in profiles with diatom DCMs in the summer, compared to profiles with no DCMs (Tripathy et al., 2015). Similarly, field studies in the Polar Antarctic Zone (PAZ) have shown that DCMs resulted in higher NPP, compared to no DCMs during summer (Parslow et al., 2001; Westwood et al., 2011). Another study (Bouman et al., 2020) found NPP estimates using a realistic non-uniform chl profile to be higher than those that did not take the vertical distribution of chlorophyll into account. At higher latitudes (~56-60°S), in situ measurements have shown low photosynthetic rates in the DCM/DBM in mid-summer (~30% of NPP), although the multi-month longevity of the DCM resulted in more downward carbon export (Boyd et al., 2024). These findings agree well with the vertical distribution of NPP recently observed in the Southern Ocean using floats, where higher NPP appears to occur below the MLD at low latitudes (30-50°S), and the depth at which 90% of NPP occurs is deeper at low latitudes (Arteaga et al., 2022).

No studies have reported NPP estimates when DCMs occur for the Southern Ocean on a large scale. Boyd et al. (2024) found that NPP in the DCMs accounted for up to 20mmol C $m^{-2}$ $day^{-1}$, and was ~0.5 µmol $L^{-1}$ $d^{-1}$ lower than in the ML. The iron and silicate-fuelled DCMs lasted ~3 months during the austral summer and their decline was linked to a decrease in light availability. We investigated profiles from a float at 54-56°S, and 140-141°E (float no. 5905371), to compare our estimates to Boyd et al., and likewise found that $NPP_{SUB}$ contributed to 18-24% of the total NPP, with most occurring in the ML during the summer of 2020-2021. We examined this float and observed that the contribution of $NPP_{SUB}$ varied significantly between the five annual cycles of data available (Figure S15), along the same latitude, ~55°S (Figure S15f). On average $\%NPP_{SUB}$ is <20% across all profiles. This is consistent with our general results, where we show that the occurrence and $\%NPP_{SUB}$ is lowest at mid-latitudes (40-60°S) and high latitudes (>60°S), where $\%NPP_{SUB}$ has a strong seasonality potentially linked to the availability of iron and silicate. This year also seems to have a longer bloom, compared to the preceding years.

## 4.3. How does DCM occurrence relate to light and iron limitation?

### 4.3.1. Light acclimation in DCM formation

We observe more and deeper DCMs, along with more DBMs, at low latitudes, and they are relatively more productive, due to more light being available there compared to higher latitudes (Figure S14). DCMs in nitrate-limited waters at low latitudes tend to be photoacclimating DCMs, following the typical DCM model for oligotrophic waters (Cullen, 2015). Photoacclimation is a well-established mechanism of DCM formation in the northern hemisphere (Richardson et al., 2000; Durham and Stocker, 2012; Cullen, 2015), where phytoplankton adapt to low light levels at depth by increasing their chl content (Geider et al., 1997; Westberry et al., 2016; Graff et al., 2019). Many northern hemisphere studies have documented DCM formation as a way for phytoplankton to access nutrients at depth when light is sufficient (Richardson and Bendtsen, 2019), while Southern Ocean studies have been added more recently (Baldry et al., 2020; Cornec et al. 2021; Boyd et al. 2024). DCMs at low latitudes are formed by phytoplankton species capable of utilising episodic supplies of nutrients. At low latitudes in oligotrophic waters, light at the DCM tends to be higher than at high latitudes because of persistent low nitrate concentrations at the surface, limiting phytoplankton growth at shallow depths. These DCMs thus follow the classic formation model of optimizing access to light and nitrate in the northern hemisphere (Cullen, 2015; Richardson and Bendtsen, 2019). We find that 64.3% of DCMs are also DBMs, so the chlorophyll peak coincides with an actual biomass peak and is not just caused by photoacclimation.

### 4.3.2. Iron limitation and DCM formation

Generally, DCMs form at or below the pycnocline, where there is sufficient light at depth and phytoplankton can be close to the nitracline (Bathmann et al., 1997; Cailliau et al., 1999; Quéguiner, 2001), as observed in the temperate North Atlantic (Richardson and Bendtsen,

2019) and oligotrophic regions (Richardson and Bendtsen, 2017). Compared to the tropics, Southern Ocean DCMs are generally deeper (64m vs. 37m depth), less intense (1.4 vs. 2.4 mg chl $m^{-3}$), shorter lived (<3 months), and are most prevalent in the summer (Cornec et al., 2021). We find that $DCM_z$ is deeper when total NPP(ALL) is low and light is higher at the $DCM_z$ (Figure S14, Figure 8a), especially in the north (<50°S), suggesting that some DCMs follow a similar DCM formation mechanism as in the northern hemisphere, where phytoplankton grow in deeper layers to access higher nutrient concentrations at depth (Richardson et al., 2000; Cullen, 2015). While this mechanism may work well in nitrate-limited regions at low latitudes like in the STZ (~30-40°S), where the nitracline sits near the MLD (Tagliabue et al., 2014; Cornec et al., 2021a), it doesn't explain DCM formation in iron-limited waters, where the average depth of the ferricline is ~333m (Tagliabue et al., 2014).

We observe widespread DCMs and DBMs, including in HNLC areas, where iron is limiting. We also see that $NPP_{SUB}$ accounts for ~40% of the total NPP at higher latitudes (<60°S) in the spring, where surface $NO_3$ is high, light is low (compared to summer months) and DCMs are shallower than at low latitudes (Figure S14). Previous studies suggested that phytoplankton may grow at great depths as a result of a nutrient supply, with aggregations of low light and low iron-adapted diatoms in deeper waters often dominating Southern Ocean DCMs (Parslow et al., 2001; Kopczynska et al., 2001; Armand et al., 2008; Gomi et al., 2007; 2010; Westwood et al., 2011; Tripathy et al., 2015). Most recently, the formation of diatom-rich DCMs and DBMs below the MLD has been linked to subsurface peaks of ammonium and a supply of recycled iron (Boyd et al., 2024). Boyd et al. propose a dual mechanism where DCMs and DBMs form as a result of iron recycling within the subsurface ammonium maxima and an upwelling of silicate, which sustains the diatom community at depth. Diatoms are known for their ability to survive and adapt to low light conditions (Strzepek et al. 2012; 2019), making it possible for them to thrive at these DCMs that form in the Southern Ocean. We find that DCMs are productive across the Southern Ocean, especially in terms of absolute numbers, regardless of the mechanism of formation.

### 4.4. What do our findings mean for satellite estimates of NPP?

Our study indicates that current satellite productivity algorithms like the CbPM require further refinement to accurately estimate NPP in the presence of DCMs. While the ferricline version of the CbPM performs reasonably well overall when DCMs are present, some important discrepancies remain. When using the ferricline, satellite estimates are closer to float values, although still differ at low and high latitudes. At low latitudes, where DCMs are more prevalent, both adaptations of the CbPM significantly overestimate NPP (Figure S13). Satellite subsurface NPP estimates, using both nitracline and ferricline approaches, are significantly higher than float-based NPP values below the MLD (Figure S13). This overestimation is driven by elevated chl:$C_{phyto}$ ratios predicted by the CbPM, creating an artificial DCM that does not match the actual DCM in the float profile. While the CbPM performs better with the ferricline approach at high latitudes, it still needs refinement for precise subsurface NPP representation at lower latitudes.

Other satellite algorithms like the Vertically Generalized Production Model (VGPM) or the Carbon, Absorption, and Fluorescence Euphotic (CAFE) model, underestimate and overestimate NPP, respectively, compared to the CbPM, especially in the Southern Ocean (Figure 2 in Westberry et al., 2023). Spatially, the CbPM tends to have higher NPP estimates particularly in the northern hemisphere. When comparing the VGPM and the CAFE to our DCM-removed profiles (<1000 mg C $m^{-2}$ $day^{-1}$), the CAFE seems to have higher estimates (500-1300 mg C $m^{-2}$ $day^{-1}$), whereas the VGPM has lower estimates overall (200-900 mg C $m^{-2}$ $day^{-1}$). However, both the VGPM and the CAFE have NPP estimates closer to the DCM-removed profiles, than the DCM profiles.

Our results clearly show that DCMs make a significant contribution to NPP, and that satellite algorithms could quantify them better. Future improvements should focus on incorporating more detailed vertical profiles and integrating data or climatologies from BGC-Argo floats. Adapting the ferricline depth based on regional and seasonal variations in the Southern Ocean could address limitations observed at low latitudes. Refining these algorithms will enhance our understanding of global NPP dynamics and improve model predictions of climate change impacts on ocean primary production.

## 5. Conclusions and implications

The importance of DCMs and their influence on NPP have never been quantified at the scale of the Southern Ocean. With the SOCCOM-led introduction of a large array of BGC-Argo floats, we are now able to better study bio-optical properties and the vertical structure of phytoplankton features basin-wide, through the seasons. Here, we have quantified the contribution of subsurface NPP to total NPP, and the effect of DCMs and DBMs on these estimates.

The significant contribution of subsurface NPP to total NPP when DCMs and DBMs are present indicates that DCMs are of biological and ecological importance in the Southern Ocean. When DCMs are present, subsurface NPP contributes more than half of the total NPP, predominantly at low latitudes north of 40°S throughout the year, from 40% in winter to 70% in the summer. At mid and high latitudes, this contribution presents a strong seasonality, decreasing from ~40% in spring to ~25% in summer. NPP at the DCM contributes up to ~20% to the total NPP annually. DCMs are especially important at low latitudes, and in summer. The contribution of subsurface NPP is higher when a DCM coincides with a DBM, and both are widespread. Satellite estimates that do not account for DCMs may be underestimating NPP by 34-45% when DCMs occur.

Most climate models primarily focus on upper ocean processes, where a decrease in phytoplankton biomass is the result of a decrease in the upward supply of nutrients (Bopp et al., 2001; Steinacher et al., 2010). Some models suggest that warmer temperatures and increased nutrient limitation may disadvantage diatoms and result in a shift towards smaller phytoplankton (Bopp et al., 2005; Marinov et al., 2010). In general, ocean circulation models show that warming will influence nutrient cycling and ocean productivity through enhanced stratification (Rhein et al., 2013; Bindoff et al., 2019; IPCC, Fifth Assessment Report AR5). Interestingly, while CMIP6 models project a global decline of 4-11% in NPP (Longhurst, 2007; Cullen, 2015; Laufkötter et al., 2015; Kwiatkowski et al. 2020), an increase in NPP is predicted specifically in the Southern Ocean (Bopp et al., 2013; Laufkötter et al., 2015). Ocean models also show large uncertainty in future projections due to insufficient regional observations and knowledge gaps in the magnitude and spatial and vertical variability of NPP (Tagliabue et al., 2021). Models are often compared against satellite products and use these as input data when observations are scarce (Aumont et al. 2015), highlighting the need to improve satellite algorithms and estimates, as these are currently the most viable method to study long-term changes on a global scale.

DCMs are often observed in stratified waters (Cullen, 2015; Carranza et al., 2018), thus, if the oceans become warmer and more stratified (Li et al., 2020), the vertical distribution of biomass will change, and the occurrence of DCMs may increase. It is therefore important to understand what effect DCMs have on the vertical distribution of NPP, particularly in the Southern Ocean, where no particular attention has been paid to DCMs (Arteaga et al., 2022; Bock et al., 2022). The lack of attention paid to DCMs and DBMs has in part been due to a lack of data with sufficient spatial coverage. Our results show that accounting for subsurface accumulations of chlorophyll and biomass matters when estimating total NPP. While the CbPM creates artificial DCMs and overestimates NPP, other satellite algorithms could potentially be missing subsurface features and underestimating NPP in the Southern Ocean, particularly in the summer, when the contribution of DCMs in terms of productivity is highest.

**Acknowledgements**

This work was possible thanks to the publicly available data from the Southern Ocean Carbon and Climate Observations and Modelling (SOCCOM) program and the National Aeronautics and Space Administration (NASA). SOCCOM is funded by the National Science Foundation, Division of Polar Programs (NSF PLR -1425989 and OPP-1936222), supplemented by NASA, and by the International Argo Program and the NOAA programs that contribute to it. The Argo Program is part of the Global Ocean Observing System The authors would like to thank the Australian Antarctic Division (AAD), in particular Ben Raymond, for facilitating the mirroring repository. We would like to thank Dr. Lionel Arteaga and Dr. Guillaume Liniger for helping with the identification of frontal zones, as well as Dr. Lionel Arteaga and Dr. Xiaogang Xing for very helpful feedback during earlier stages of this manuscript. This research was supported by the Australian Research Council Centre of Excellence for Climate Extremes (CLEX; CE170100023). P. W. Boyd is also supported by the Australian Antarctic Program Partnership as part of the Antarctic Science Collaboration Initiative (ASCI000002).

**Author contribution statement**

CRV, CS and PGS conceived the idea for the study. CRV created the code to analyse all data with advice from JB and PGS. CRV interpreted the results with input from CS, PGS, PWB,

JB and KR. CRV wrote the first version of the manuscript with great help and constructive feedback from CS, PGS and PWB. All authors commented and contributed to the final version of the manuscript.

**Data availability statements**

BGC Argo float data were collected and made freely available by the Southern Ocean Carbon and Climate Observations and Modelling (SOCCOM) program, and by the International Argo Program and the national programs that contribute to it (https://argo.ucsd.edu, https://www.ocean-ops.org). The Argo Program is part of the Global Ocean Observing System. The PAR satellite data were obtained from the NASA Ocean Color web site (https://oceancolor.gsfc.nasa.gov). The original code for the satellite-based CbPM can be found at http://sites.science.oregonstate.edu/ocean.productivity/cbpm2.code.php.

**Conflict of interest statement**

All authors declare that they have no conflicts of interest.

**References**

Ardyna, M., Babin, M., Gosselin, M., Devred, E., Bélanger, S., Matsuoka, A., & Tremblay, J. E. (2013). Parameterization of vertical chlorophyll a in the Arctic Ocean: Impact of the subsurface chlorophyll maximum on regional, seasonal, and annual primary production estimates. *Biogeosciences*, *10*(6), 4383–4404. https://doi.org/10.5194/bg-10-4383-2013

Armand, L. K., Cornet-Barthaux, V., Mosseri, J., & Quéguiner, B. (2008). Late summer diatom biomass and community structure on and around the naturally iron-fertilised Kerguelen Plateau in the Southern Ocean. *Deep-Sea Research Part II: Topical Studies in Oceanography*, *55*(5–7), 653–676. https://doi.org/10.1016/j.dsr2.2007.12.031

Armand, L. K., Crosta, X., Quéguiner, B., Mosseri, J., & Garcia, N. (2008). Diatoms preserved in surface sediments of the northeastern Kerguelen Plateau. *Deep-Sea Research Part II: Topical Studies in Oceanography*, *55*(5–7), 677–692. https://doi.org/10.1016/j.dsr2.2007.12.032

Arteaga, L. A., Pahlow, M., Bushinsky, S. M., & Sarmiento, J. L. (2019). Nutrient controls on export production in the Southern Ocean. *Global Biogeochemical Cycles*, *33*(8), 942-

956.

Arteaga, L. A., Boss, E., Behrenfeld, M. J., Westberry, T. K., & Sarmiento, J. L. (2020). Seasonal modulation of phytoplankton biomass in the Southern Ocean. *Nature Communications*, *11*(1). https://doi.org/10.1038/s41467-020-19157-2

Arteaga, L. A., Behrenfeld, M. J., Boss, E., & Westberry, T. K. (2022). Vertical Structure in Phytoplankton Growth and Productivity Inferred From Biogeochemical-Argo Floats and the Carbon-Based Productivity Model. *Global Biogeochemical Cycles*, *36*(8), 1–20. https://doi.org/10.1029/2022GB007389

Aumont, O., Éthé, C., Tagliabue, A., Bopp, L., & Gehlen, M. (2015). PISCES-v2: an ocean biogeochemical model for carbon and ecosystem studies. *Geoscientific Model Development Discussions*, *8*(2), 1375-1509.

Baldry, K., Strutton, P. G., Hill, N. A., & Boyd, P. W. (2020). Subsurface Chlorophyll-a Maxima in the Southern Ocean. *Frontiers in Marine Science*, *7*(August). https://doi.org/10.3389/fmars.2020.00671

Barbieux, M., Uitz, J., Gentili, B., Pasqueron De Fommervault, O., Mignot, A., Poteau, A., … Bricaud, A. (2019). Bio-optical characterization of subsurface chlorophyll maxima in the Mediterranean Sea from a Biogeochemical-Argo float database. *Biogeosciences*, *16*(6), 1321–1342. https://doi.org/10.5194/bg-16-1321-2019

Bathmann, U. V., Scharek, R., Klaas, C., Dubischar, C. D., & Smetacek, V. (1997). Spring development of phytoplankton biomass and composition in major water masses of the Atlantic sector of the Southern Ocean. *Deep-Sea Research Part II: Topical Studies in Oceanography*, *44*(1–2), 51–67. https://doi.org/10.1016/S0967-0645(96)00063-X

Behrenfeld, M. J., Boss, E., Siegel, D. A., & Shea, D. M. (2005). Carbon-based ocean productivity and phytoplankton physiology from space. *Global Biogeochemical Cycles*, *19*(1), 1–14. https://doi.org/10.1029/2004GB002299

Behrenfeld, M. J., & Falkowski, P. G. (1997a). A consumer's guide to phytoplankton primary productivity models. *Limnology and Oceanography*, *42*(7), 1479–1491. https://doi.org/10.4319/lo.1997.42.7.1479

Behrenfeld, M. J., & Falkowski, P. G. (1997b). Photosynthetic rates derived from satellite-based chlorophyll concentration. *Limnology and Oceanography*, *42*(1), 1–20. https://doi.org/10.4319/lo.1997.42.1.0001

Bendtsen, J., Vives, C. R., & Richardson, K. (2023). Primary production in the North Atlantic estimated from in situ water column data observed by Argo fl oats and remote sensing. *Frontiers in Marine Science*, (January), 1–13.

https://doi.org/10.3389/fmars.2023.1062413

Bindoff, N. L., Cheung, W. W., Kairo, J. G., Arístegui, J., Guinder, V. A., Hallberg, R., ... & Williamson, P. (2019). Changing Ocean, Marine Ecosystems, and Dependent Communities. *IPCC Special Report on the Ocean and Cryosphere in a Changing Climate*, 477–587.

Bittig, H. C., Maurer, T. L., Plant, J. N., Schmechtig, C., Wong, A. P. S., Claustre, H., … Xing, X. (2019). A BGC-Argo Guide: Planning, Deployment, Data Handling and Usage. *Frontiers in Marine Science*, *6*(August). https://doi.org/10.3389/fmars.2019.00502

Bock, N., Cornec, M., Claustre, H., & Duhamel, S. (2022). Biogeographical Classification of the Global Ocean From BGC-Argo Floats. *Global Biogeochemical Cycles*, *36*(6), 1–24. https://doi.org/10.1029/2021GB007233

Bopp, L., Resplandy, L., Orr, J. C., Doney, S. C., Dunne, J. P., Gehlen, M., … Vichi, M. (2013). Multiple stressors of ocean ecosystems in the 21st century: Projections with CMIP5 models. *Biogeosciences*, *10*(10), 6225–6245. https://doi.org/10.5194/bg-10-6225-2013

Bopp, L, Aumont, O., Cadule, P., Alvain, S., & Gehlen, M. (2005). Response of diatoms distribution to global warming and potential implications : A global model study, *32*(October), 2–5. https://doi.org/10.1029/2005GL023653

Bopp, Laurent, Monfray, P., Aumont, O., Dufresne, J. L., Le Treut, H., Madec, G., … Orr, J. C. (2001). Potential impact of climate change on marine export production. *Global Biogeochemical Cycles*, *15*(1), 81–99. https://doi.org/10.1029/1999GB001256

Boss, E. B., & Haëntjens, N. (2016). SOCCOM Technical Report Series. Primer regarding measurements of chlorophyll fluorescence and the backscattering coefficient with WETLabs FLBB on profiling floats. Retrieved from http://soccom.princeton.edu

Bouman, H. A., Jackson, T., Sathyendranath, S., & Platt, T. (2020). Vertical structure in chlorophyll profiles: influence on primary production in the Arctic Ocean. *Philosophical Transactions of the Royal Society A*, *378*(2181), 20190351.

Boyd, P. W., Jickells, T., Law, C. S., Blain, S., Boyle, E. A., Buesseler, K. O., ... & Watson, A. J. (2007). Mesoscale iron enrichment experiments 1993-2005: synthesis and future directions. *science*, *315*(5812), 612-617.

Boyd, P. W., & Trull, T. W. (2007). Understanding the export of biogenic particles in oceanic waters: Is there consensus? *Progress in Oceanography*, *72*(4), 276–312. https://doi.org/10.1016/j.pocean.2006.10.007

Boyd, P. W. (2015). Toward quantifying the response of the oceans' biological pump to climate change. *Frontiers in Marine Science*, *2*(October), 1–15. https://doi.org/10.3389/fmars.2015.00077

Boyd, P. W., Antoine, D., Baldry, K., Cornec, M., Ellwood, M., Halfter, S., Lacour, L., Latour, P., Strzepek, R.F., Trull, T.W. and Rohr, T. (2024). Controls on Polar Southern Ocean Deep Chlorophyll Maxima: Viewpoints from multiple observational platforms. *Global Biogeochemical Cycles*, *38*(3), e2023GB008033.

Briggs, N., Perry, M. J., Cetinić, I., Lee, C., D'Asaro, E., Gray, A. M., & Rehm, E. (2011). High-resolution observations of aggregate flux during a sub-polar North Atlantic spring bloom. *Deep-Sea Research Part I: Oceanographic Research Papers*, *58*(10), 1031–1039. https://doi.org/10.1016/j.dsr.2011.07.007

Brown, Z. W., Lowry, K. E., Palmer, M. A., van Dijken, G. L., Mills, M. M., Pickart, R. S., & Arrigo, K. R. (2015). Characterizing the subsurface chlorophyll a maximum in the Chukchi Sea and Canada Basin. *Deep Sea Research Part II: Topical Studies in Oceanography*, *118*, 88-104.

Bushinsky, S. M., Gray, A. R., Johnson, K. S., & Sarmiento, J. L. (2017). Oxygen in the Southern Ocean from Argo floats: Determination of processes driving air-sea fluxes. *Journal of Geophysical Research: Oceans*, *122*(11), 8661-8682.

Cailliau, C., Belviso, S., Goutx, M., Bedo, A., Park, Y., & Charriaud, E. (1999). Sedimentation pathways in the Indian sector of the Southern Ocean during a production regime dominated by regeneration. *Marine Ecology Progress Series*, *190*, 53–67. https://doi.org/10.3354/meps190053

Carranza, M. M., Gille, S. T., Franks, P. J. S., Johnson, K. S., Pinkel, R., & Girton, J. B. (2018). When mixed layers are not mixed. Storm-driven mixing and bio-optical vertical gradients in mixed layers of the Southern Ocean. *Journal of Geophysical Research: Oceans*, 7264–7289. https://doi.org/10.1029/2018JC014416

Cornec, M., Claustre, H., Mignot, A., Guidi, L., Lacour, L., Poteau, A., … Schmechtig, C. (2021a). Deep Chlorophyll Maxima in the Global Ocean: Occurrences, Drivers and Characteristics. *Global Biogeochemical Cycles*, *35*(4), 1–30. https://doi.org/10.1029/2020GB006759

Cornec, M., Laxenaire, R., Speich, S., & Claustre, H. (2021b). Impact of mesoscale eddies on deep chlorophyll maxima. *Geophysical Research Letters*, *48*(15), e2021GL093470.

Cullen, J. J. (1982). The deep chlorophyll maximum: comparing vertical profiles of chlorophyll a. *Canadian Journal of Fisheries and Aquatic Sciences*, *39*(5), 791–803. https://doi.org/10.1139/f82-108

Cullen, J. J., & Lewis, M. R. (1995). Biological processes and optical measurements near the sea surface: some issues relevant to remote sensing. *Journal of Geophysical Research*, *100*(C7). https://doi.org/10.1029/95jc00454

Cullen, John J. (2015). Subsurface chlorophyll maximum layers: Enduring enigma or mystery solved? *Annual Review of Marine Science, 7*, 207–239. https://doi.org/10.1146/annurev-marine-010213-135111

de Boyer Montégut, C., Madec, G., Fischer, A. S., Lazar, A., & Iudicone, D. (2004). Mixed layer depth over the global ocean: An examination of profile data and a profile-based climatology. *Journal of Geophysical Research C: Oceans*, *109*(12), 1–20. https://doi.org/10.1029/2004JC002378

Durham, W. M., & Stocker, R. (2012). Thin phytoplankton layers: characteristics, mechanisms, and consequences. *Annual review of marine science*, *4*(1), 177-207.

Estapa, M. L., Feen, M. L., & Breves, E. (2019). Direct Observations of Biological Carbon Export From Profiling Floats in the Subtropical North Atlantic. *Global Biogeochemical Cycles*, *33*(3), 282–300. https://doi.org/10.1029/2018GB006098

Estrada, M., Marrasé, C., Latasa, M., Berdalet, E., Delgado, M., Estrada, M., … Riera, T. (1993). Variability of deep chlorophyll maximum characteristics in the Northwestern Mediterranean. *Marine Ecology Progress Series*, 289–300.

Fawcett, S. E., Lomas, M. W., Ward, B. B., & Sigman, D. M. (2014). The counterintuitive effect of summer-to-fall mixed layer deepening on eukaryotic new production in the Sargasso Sea. *Global Biogeochemical Cycles*, *28*, 86–102. https://doi.org/10.1002/2013GB004579.Received

Fennel, K., & Boss, E. (2003). Subsurface maxima of phytoplankton and chlorophyll: Steady-state solutions from a simple model. *Limnology and Oceanography*, *48*(4), 1521–1534. https://doi.org/10.4319/lo.2003.48.4.1521

Field, C. B., Behrenfeld, M. J., Randerson, J. T., & Falkowski, P. (1998). Primary production of the biosphere: Integrating terrestrial and oceanic components. *Science*, *281*(5374), 237–240. https://doi.org/10.1126/science.281.5374.237

Geider, R. J., MacIntyre, H. L., & Kana, T. M. (1997). Dynamic model of phytoplankton growth and acclimation: responses of the balanced growth rate and the chlorophyll a: carbon ratio to light, nutrient-limitation and temperature. *Marine Ecology Progress Series*, *148*, 187-200.

Geider, R. J., Maclntyre, H. L., & Kana, T. M. (1998). A dynamic regulatory model of phytoplanktonic acclimation to light, nutrients, and temperature. *Limnology and* *oceanography*, *43*(4), 679-694.

Gomi, Y., Fukuchi, M., & Taniguchi, A. (2010). Diatom assemblages at subsurface chlorophyll maximum layer in the eastern Indian sector of the Southern Ocean in summer. *Journal of Plankton Research*, *32*(7), 1039–1050. https://doi.org/10.1093/plankt/fbq031

Gomi, Y., Taniguchi, A., & Fukuchi, M. (2007). Temporal and spatial variation of the phytoplankton assemblage in the eastern Indian sector of the Southern Ocean in summer 2001/2002. *Polar Biology*, *30*(7), 817–827. https://doi.org/10.1007/s00300-006-0242-2

Graff, J. R., Westberry, T. K., Milligan, A. J., Brown, M. B., Dall'Olmo, G., van Dongen-Vogels, V., … Behrenfeld, M. J. (2015). Analytical phytoplankton carbon measurements spanning diverse ecosystems. *Deep-Sea Research Part I: Oceanographic Research Papers*, *102*, 16–25. https://doi.org/10.1016/j.dsr.2015.04.006

Graff, J. R., Westberry, T. K., Milligan, A. J., Brown, M. B., Olmo, G. D., Reifel, K. M., & Behrenfeld, M. J. (2016). Photoacclimation of natural phytoplankton communities. *Marine Ecology Progress Series*, *542*, 51-62.

Gruber, N., Clement, D., Carter, B. R., Feely, R. A., van Heuven, S., Hoppema, M., … Wanninkhof, R. (2019). The oceanic sink for anthropogenic CO 2 from 1994 to 2007. *Science*, *363*(6432), 1193–1199. https://doi.org/10.1126/science.aau5153

Gruber, N., Landschutzer, P., & Lovenduski, N. S. (2019). The Variable Southern Ocean Carbon Sink. *Science Advances*, *11*, 159–186. https://doi.org/10.1126/sciadv.aav6471

Henson, S. A., Sanders, R., & Madsen, E. (2012). Global patterns in efficiency of particulate organic carbon export and transfer to the deep ocean. *Global Biogeochemical Cycles*, *26*(1), 1–14. https://doi.org/10.1029/2011GB004099

Hickman, A. E., Moore, C. M., Sharples, J., Lucas, M. I., Tilstone, G. H., Krivtsov, V., & Holligan, P. M. (2012). Primary production and nitrate uptake within the seasonal thermocline of a stratified shelf sea. *Marine Ecology Progress Series*, *463*, 39–57. https://doi.org/10.3354/meps09836

Hiscock, M. R., Marra, J., Smith Jr, W. O., Goericke, R., Measures, C., Vink, S., ... & Barber, R. T. (2003). Primary productivity and its regulation in the Pacific Sector of the Southern Ocean. *Deep Sea Research Part II: Topical Studies in Oceanography*, *50*(3-4), 533-558.

Holte, J., & Talley, L. (2009). A new algorithm for finding mixed layer depths with applications to argo data and subantarctic mode water formation. *Journal of Atmospheric and Oceanic Technology*, *26*(9), 1920–1939.

https://doi.org/10.1175/2009JTECHO543.1

Huang, Y., Nicholson, D., Huang, B., & Cassar, N. (2021). Global Estimates of Marine Gross Primary Production Based on Machine Learning Upscaling of Field Observations. *Global Biogeochemical Cycles*, *35*(3), 1–18. https://doi.org/10.1029/2020GB006718

Johnson, K. S., Plant, J. N., Dunne, J. P., Talley, L. D., & Sarmiento, J. L. (2017). Annual nitrate drawdown observed by SOCCOM profiling floats and the relationship to annual net community production. *Journal of Geophysical Research: Oceans*, *122*(8), 6668–6683. https://doi.org/10.1002/2017JC012839

Kopczynska, E. E., Dehairs, F., Elskens, M., & Wright, S. (2001). Phytoplankton and microzooplankton variability between the Subtropical and Polar Fronts south of Australia: Thriving under regenerative and new production in late summer. *Journal of Geophysical Research: Oceans*, *106*(C12), 31597–31609. https://doi.org/10.1029/2000jc000278

Kwiatkowski, L., Torres, O., Bopp, L., Aumont, O., Chamberlain, M., Christian, J. R., ... & Ziehn, T. (2020). Twenty-first century ocean warming, acidification, deoxygenation, and upper-ocean nutrient and primary production decline from CMIP6 model projections. Biogeosciences, 17(13), 3439-3470.

Lacour, L., Ardyna, M., Stec, K. F., Claustre, H., Prieur, L., Poteau, A., … Iudicone, D. (2017). Unexpected winter phytoplankton blooms in the North Atlantic subpolar gyre. *Nature Geoscience*, *10*(11), 836–839. https://doi.org/10.1038/NGEO3035

Latasa, M., Cabello, A. M., Morán, X. A. G., Massana, R., & Scharek, R. (2017). Distribution of phytoplankton groups within the deep chlorophyll maximum. *Limnology and Oceanography*, *62*(2), 665–685. https://doi.org/10.1002/lno.10452

Latasa, M., Gutiérrez-Rodríguez, A., Cabello, A. M. M., & Scharek, R. (2016). Influence of light and nutrients on the vertical distribution of marine phytoplankton groups in the deep chlorophyll maximum. *Scientia Marina*, *80*(S1), 57–62. https://doi.org/10.3989/scimar.04316.01a

Laufkötter, C., Vogt, M., Gruber, N., Aita-Noguchi, M., Aumont, O., Bopp, L., … Volker, C. (2015). Drivers and uncertainties of future global marine primary production in marine ecosystem models. *Biogeosciences*, *12*(23), 6955–6984. https://doi.org/10.5194/bg-12-6955-2015

Laws, E. A., Letelier, R. M., & Karl, D. M. (2014). Estimating the compensation irradiance in the ocean: The importance of accounting for non-photosynthetic uptake of inorganic carbon. *Deep Sea Research Part I: Oceanographic Research Papers*, *93*, 35-40.

Letelier, R. M., Karl, D. M., Abbott, M. R., & Bidigare, R. R. (2004). Light driven seasonal patterns of chlorophyll and nitrate in the lower euphotic zone of the North Pacific Subtropical Gyre. *Limnology and Oceanography*, *49*(2), 508–519. https://doi.org/10.4319/lo.2004.49.2.0508

Li, G., Cheng, L., Zhu, J., Trenberth, K. E., Mann, M. E., & Abraham, J. P. (2020). Increasing ocean stratification over the past half-century. *Nature Climate Change*, *10*(12), 1116-1123.

Liniger, G., Moreau, S., Lannuzel, D., & Strutton, P. (2024). Large contribution of the sea-ice zone to Southern Ocean carbon export revealed by BGC-Argo floats. *Pre-print, Version 2, posted 03 Apr, 2024. Accessed on 8, July, 2024*.

Llort, J., Langlais, C., Matear, R., Moreau, S., Lenton, A., & Strutton, P. G. (2018). Evaluating Southern Ocean carbon eddy-pump from biogeochemical-Argo floats. *Journal of Geophysical Research: Oceans*, *123*(2), 971-984.

Long, J. S., Fassbender, A. J., & Estapa, M. L. (2021). Depth-resolved net primary production in the Northeast Pacific Ocean: A comparison of satellite and profiling float estimates in the context of two marine heatwaves. *Geophysical Research Letters*, *48*(19), e2021GL093462.

Longhurst, A. (2007). *Ecological Geography of the Sea*. https://doi.org/10.1016/0079-6611(95)00015-1

Longhurst, A., Sathyendranath, S., Platt, T., & Caverhill, C. (1995). An estimate of global primary production in the ocean from satellite radiometer data. *Journal of Plankton Research*, *17*(6), 1245–1271. https://doi.org/10.1093/plankt/17.6.1245

Marañón, E., Van Wambeke, F., Uitz, J., Boss, E. S., Dimier, C., Dinasquet, J., ... & Zäncker, B. (2021). Deep maxima of phytoplankton biomass, primary production and bacterial production in the Mediterranean Sea. *Biogeosciences*, *18*(5), 1749-1767.

Marinov, I., Doney, S. C., & Lima, I. D. (2010). Response of ocean phytoplankton community structure to climate change over the 21st century: Partitioning the effects of nutrients, temperature and light. *Biogeosciences*, *7*(12), 3941–3959. https://doi.org/10.5194/bg-7-3941-2010

Martin, J. H., Gordon, R. M., & Fitzwater, S. E. (1990). Iron in Antarctic waters. *Nature*, *345*(6271), 156-158.

McDougall, T. J., & Barker, P. M. (2011). *Getting started with TEOS-10 and the Gibbs Seawater ( GSW ). Scor/Iapso Wg127*. Retrieved from http://www.teos-10.org/pubs/gsw/v3_04/pdf/Getting_Started.pdf

Mignot, A., Claustre, H., Uitz, J., Poteau, A., D'Ortenzio, F., & Xing, X. (2014). Understanding the seasonal dynamics of phytoplankton biomass and the deep chlorophyll maximum in oligotrophic environments: A Bio-Argo float investigation. *Global Biogeochemical Cycles*, *28*, 856–876. https://doi.org/10.1111/1462-2920.13280

Morel, A. (1988). Optical modeling of the upper ocean in relation to its biogenous matter content (case I waters). *Journal of Geophysical Research*, *93*(C9), 10749. https://doi.org/10.1029/jc093ic09p10749

Morel, A., Huot, Y., Gentili, B., Werdell, P. J., Hooker, S. B., & Franz, B. A. (2007). Examining the consistency of products derived from various ocean color sensors in open ocean (Case 1) waters in the perspective of a multi-sensor approach. *Remote Sensing of Environment*, *111*(1), 69–88. https://doi.org/10.1016/j.rse.2007.03.012

Morel, A., & Maritorena, S. (2001). Bio-optical properties of oceanic waters: A reappraisal. *Journal of Geophysical Research: Oceans*, *106*(C4), 7163–7180. https://doi.org/10.1029/2000jc000319

Parslow, J. S., Boyd, P. W., Rintoul, S. R., & Griffiths, F. B. (2001). A persistent subsurface chlorophyll maximum in the Interpolar Frontal Zone south of Australia: Seasonal progression and implications for phytoplankton-light-nutrient interactions. *Journal of Geophysical Research: Oceans*, *106*(C12), 31543–31557. https://doi.org/10.1029/2000jc000322

Pinkerton, M. H., Boyd, P. W., Deppeler, S., Hayward, A., Höfer, J., & Moreau, S. (2021). Evidence for the impact of climate change on primary producers in the Southern Ocean. *Frontiers in Ecology and Evolution*, *9*, 592027.

Platt, T., Sathyendranath, S., Caverhill, C., & Lewis, M. R. (1988). Ocean primary production and available light: further algorithms for remote sensing, *35*(6), 855–879.

Quéguiner, B. (2001). Biogenic silica production in the Australian sector of the Subantarctic Zone of the Southern Ocean in late summer 1998. *Journal of Geophysical Research: Oceans*, *106*(C12), 31627–31636. https://doi.org/10.1029/2000jc000249

Rhein, M., Rintoul, S. R., Aoki, S., Campos, E., Chambers, D., Feely, R. A., … Wang, F. (2013). Observations: Ocean. In: Climate Change 2013: The Physical Science Basis. Contribution of Working Group I to the Fifth Assessment Report of the Intergovernmental Panel on Climate Change [Stocker, T.F., D. Qin, G.-K. Plattner, M. Tignor, S.K. Allen, J. Bos. *Cambridge University Press, Cambridge, United Kingdom and New York, NY, USA, 2013.*

Richardson, K., Visser, A. W., & Pedersen, F. B. (2000). Subsurface phytoplankton blooms fuel pelagic production in the North Sea. *Journal of Plankton Research*, *22*(9), 1663–1671. https://doi.org/10.1093/plankt/22.9.1663

Richardson, Katherine, & Bendtsen, J. (2019). Vertical distribution of phytoplankton and primary production in relation to nutricline depth in the open ocean. *Marine Ecology Progress Series*, *620*, 33–46. https://doi.org/10.3354/meps12960

Richardson, Katherine, Bendtsen, J., Christensen, J. T., Adjou, M., Lyngsgaard, M. M., Hilligsøe, K. M., … Nielsen, M. H. (2014). Localised mixing and heterogeneity in the plankton food web in a frontal region of the Sargasso Sea: Implications for eel early life history? *Marine Ecology Progress Series*, *504*, 91–107. https://doi.org/10.3354/meps10766

Roesler, C., Uitz, J., Claustre, H., Boss, E., Xing, X., Organelli, E., … Barbieux, M. (2017). Recommendations for obtaining unbiased chlorophyll estimates from in situ chlorophyll fluorometers: A global analysis of WET Labs ECO sensors. *Limnology and Oceanography: Methods*, *15*(6), 572–585. https://doi.org/10.1002/lom3.10185

Schallenberg, C., Strzepek, R. F., Bestley, S., Wojtasiewicz, B., & Trull, T. W. (2022). Iron Limitation Drives the Globally Extreme Fluorescence/Chlorophyll Ratios of the Southern Ocean. *Geophysical Research Letters*, *49*(12). https://doi.org/10.1029/2021gl097616

Schmechtig, C., Poteau, A., Claustre, H., D’Ortenzio, F., & Boss, E. (2015). Processing Bio-Argo chlorophyll-a concentration at the DAC Level. *Argo Data Management*, 1–22. http://doi.org/10.13155/39468

Silsbe, G. M., & Malkin, S. Y. (2016). *Where light and nutrients collide: The global distribution and activity of subsurface chlorophyll maximum layers.* (Aquatic microbial ecology and biogeochemistry: A dual perspective, Ed.).

Steinacher, M., Joos, F., Frölicher, T. L., Bopp, L., Cadule, P., Cocco, V., … Segschneider, J. (2010). Projected 21st century decrease in marine productivity: A multi-model analysis. *Biogeosciences*, *7*(3), 979–1005. https://doi.org/10.5194/bg-7-979-2010

Strutton, P. G., Trull, T. W., Phillips, H. E., Duran, E. R., & Pump, S. (2023). Biogeochemical Argo floats reveal the evolution of subsurface chlorophyll and particulate organic carbon in southeast Indian Ocean eddies. *Journal of Geophysical Research: Oceans*, *128*(4), e2022JC018984.

Strzepek, R. F., Hunter, K. A., Frew, R. D., Harrison, P. J., & Boyd, P. W. (2012). Iron-light interactions differ in Southern Ocean phytoplankton. *Limnology and Oceanography*, *57*(4), 1182-1200.

Strzepek, R. F., Boyd, P. W., & Sunda, W. G. (2019). Photosynthetic adaptation to low iron, light, and temperature in Southern Ocean phytoplankton. *Proceedings of the National Academy of Sciences*, *116*(10), 4388-4393.

Su, J., Strutton, P. G., & Schallenberg, C. (2021). The subsurface biological structure of Southern Ocean eddies revealed by BGC-Argo floats. *Journal of Marine Systems*, *220*(April), 103569. https://doi.org/10.1016/j.jmarsys.2021.103569

Su, J., Schallenberg, C., Rohr, T., Strutton, P. G., & Phillips, H. E. (2022). New estimates of Southern Ocean annual net community production revealed by BGC-Argo floats. *Geophysical Research Letters*, *49*(15), e2021GL097372.

Tagliabue, A., Kwiatkowski, L., Bopp, L., Butenschön, M., Cheung, W., Lengaigne, M., & Vialard, J. (2021). Persistent Uncertainties in Ocean Net Primary Production Climate Change Projections at Regional Scales Raise Challenges for Assessing Impacts on Ecosystem Services. *Frontiers in Climate*, *3*(November), 1–16. https://doi.org/10.3389/fclim.2021.738224

Tagliabue, A., Sallée, J. B., Bowie, A. R., Lévy, M., Swart, S., & Boyd, P. W. (2014). Surface-water iron supplies in the Southern Ocean sustained by deep winter mixing. *Nature Geoscience*, *7*(4), 314–320. https://doi.org/10.1038/ngeo2101

Tripathy, S. C., Pavithran, S., Sabu, P., Pillai, H. U. K., Dessai, D. R. G., & Anilkumar, N. (2015). Deep chlorophyll maximum and primary productivity in Indian Ocean sector of the Southern Ocean: Case study in the Subtropical and Polar Front during austral summer 2011. *Deep-Sea Research Part II: Topical Studies in Oceanography*, *118*, 240–249. https://doi.org/10.1016/j.dsr2.2015.01.004

Trull, T., Rintoul, S. R., Hadfield, M., & Abraham, E. R. (2001). Circulation and seasonal evolution of polar waters south of Australia: Implications for iron fertilization of the Southern Ocean. *Deep Sea Research Part II: Topical Studies in Oceanography*, *48*(11-12), 2439-2466.

Uchida, T., Balwada, D., P. Abernathey, R., A. McKinley, G., K. Smith, S., & Lévy, M. (2020). Vertical eddy iron fluxes support primary production in the open Southern Ocean. *Nature Communications*, *11*(1), 1125.

Westberry, T., Behrenfeld, M. J., Siegel, D. A., & Boss, E. (2008). Carbon-based primary productivity modeling with vertically resolved photoacclimation. *Global Biogeochemical Cycles*, *22*(2), 1–18. https://doi.org/10.1029/2007GB003078

Westberry, T. K., Silsbe, G. M., & Behrenfeld, M. J. (2023). Gross and net primary production in the global ocean: An ocean color remote sensing perspective. *Earth-*

*Science Reviews*, *237*(January), 104322. https://doi.org/10.1016/j.earscirev.2023.104322

Westwood, K. J., Brian Griffiths, F., Webb, J. P., & Wright, S. W. (2011). Primary production in the Sub-Antarctic and Polar Frontal Zones south of Tasmania, Australia; SAZ-Sense survey, 2007. *Deep-Sea Research Part II: Topical Studies in Oceanography*. https://doi.org/10.1016/j.dsr2.2011.05.017

Yang, B., Fox, J., Behrenfeld, M. J., Boss, E. S., Haëntjens, N., Halsey, K. H., … Doney, S. C. (2021). In Situ Estimates of Net Primary Production in the Western North Atlantic With Argo Profiling Floats. *Journal of Geophysical Research: Biogeosciences*, *126*(2), 1–16. https://doi.org/10.1029/2020JG006116

Yang, B., Gomez, F., Schmid, C., & Baringer, M. (2022). In situ estimates of net primary production in the open-ocean Gulf of Mexico. *Limnology And Oceanography Letters*, 427–434. https://doi.org/10.1002/lol2.10270